Chemical Engineering Journal 521 (2025) 166416

Contents lists available at ScienceDirect

Chemical Engineering Journal

journal homepage: www.elsevier.com/locate/cej

Solar-assisted thermal pre-treatment of waste activated sludge in a tubular photoreactor: Operational and economic insights

Joana P. Monteiro [a,b,c], Tânia F.C.V. Silva [a,b], Catarina Cruzeiro [a,b,*], M. Salomé Duarte [c,d], M. Alcina Pereira [c,d], Vítor J.P. Vilar [a,b,*]

[a] LSRE-LCM – Laboratory of Separation and Reaction Engineering - Laboratory of Catalysis and Materials, Faculty of Engineering, University of Porto, Rua Dr. Roberto Frias, 4200-465 Porto, Portugal
[b] ALiCE – Associate Laboratory in Chemical Engineering, Faculty of Engineering, University of Porto, Rua Dr. Roberto Frias, 4200-465 Porto, Portugal
[c] CEB - Centre of Biological Engineering, University of Minho, Braga 4710-057, Portugal
[d] LABBELS – Associate Laboratory, Braga/Guimarães, Portugal

ARTICLE INFO

Keywords:
Thermal hydrolysis
Renewable energy
Tubular photoreactor
Methane production
Economic analysis

ABSTRACT

Anaerobic digestion (AD) is crucial for sludge stabilisation and biogas generation, yet its efficiency is often limited by the slow hydrolysis of waste-activated sludge (WAS). This study explores a novel pre-treatment approach that integrates low-temperature heating with solar radiation in a tubular photoreactor–comprising a borosilicate-glass tube over a reflective surface–to enhance urban WAS disintegration and boost methane production in AD. Lab-scale experiments (1 L) evaluated the effects of temperature (50–70 °C), radiant power (0.45–0.83 W_{UV}), and reflector geometries. Under simulated sunlight (0.66 W_{UV}), a 3-hour pre-treatment increased WAS disintegration by up to 17 %, enhanced EPS release, and boosted the methane production by up to 74 %, with a peak of 212 ± 6 L CH_4 kg_{VS}^{-1} at 70 °C (7.6 kJ_{UV} L^{-1}). These outcomes confirm a synergistic effect between thermal and solar energy input. Pilot-scale experiments (15 L) under natural sunlight, without external heating, confirmed an 85 % increase in methane production. Solar radiation alone raised WAS temperature from 20 to 63 °C in 4 h (16.6 kJ_{UV} L^{-1}) and sustained it for 3 more hours (12.1 kJ_{UV} L^{-1}), achieving a WAS disintegration degree of 12 %. An economic assessment compared two scenarios: 1) one relying solely on solar radiation (28.7 kJ_{UV} L^{-1}) captured by compound parabolic collectors (CPCs); and 2) another adding external heating (12.1 kJ_{UV} L^{-1}; 1672 MWh). Although external heating reduces the required CPC area, its high electricity demand diminishes economic feasibility. Consequently, scenario 1 offers a more favourable balance between capital and operating expenses, reducing total yearly costs by 23 %.

1. Introduction

Anaerobic digestion (AD) technology constitutes a chemo-biological process that reduces fossil fuel consumption by converting organic waste into biogas, a renewable energy source [1]. As a fundamental component of sustainable energy systems, AD addresses global waste management challenges while facilitating the transition to cleaner energy. Biogas, a renewable energy carrier, is increasingly recognized for its critical role in achieving energy sustainability [2,3]. Within this context, the European Union (EU) has introduced the REPowerEU strategic plan, which underscores the importance of biogas by setting an ambitious target to increase biomethane production from 3.5 to 35 billion cubic meters (approximately 350 TWh) by 2030 [4]. Simultaneously, urban wastewater treatment plants (WWTPs) must achieve energy neutrality by 2045, balancing energy consumption with renewable energy generation according to the EU Directive 2024/3019 [5]. These EU initiatives focus on improving energy efficiency and incorporating sustainable practices in WWTPs.

Despite its benefits, AD remains energy-intensive, contributing to approximately 14 % of a WWTP's total energy demand [6]. However, biogas is a valuable energy source due to its ability to store energy, which is essential for balancing supply and demand [7]. Current research focuses on advancing technologies to increase biogas production, helping WWTPs achieve energy self-sufficiency. One major

* Corresponding authors at: LSRE-LCM – Laboratory of Separation and Reaction Engineering - Laboratory of Catalysis and Materials, Faculty of Engineering, University of Porto, Rua Dr. Roberto Frias, 4200-465 Porto, Portugal.
E-mail addresses: crcruzeiro@fe.up.pt (C. Cruzeiro), vilar@fe.up.pt (V.J.P. Vilar).

https://doi.org/10.1016/j.cej.2025.166416
Received 22 April 2025; Received in revised form 14 July 2025; Accepted 23 July 2025
Available online 25 July 2025
1385-8947/© 2025 The Authors. Published by Elsevier B.V. This is an open access article under the CC BY-NC-ND license (http://creativecommons.org/licenses/by-nc-nd/4.0/).

challenge is the complex composition of waste-activated sludge (WAS), characterized by floc structures, rigid cell walls, and high-molecular-weight organic matter, which limit the efficiency of the hydrolysis step in AD [8]. To tackle this issue, pre-treatment methods are used to break down the complex structure of sludge. These methods are generally classified into four categories: physical, biological, chemical, and combined pre-treatments [9].

Among physical methods, thermal pre-treatment is highly effective due to its ability to disrupt chemical bonds in cell walls and membranes, releasing intracellular components for biological degradation [10,11]. High-temperature pre-treatment, typically operated at temperatures above 100 °C under pressure, has been successfully implemented at full scale [9,12]. The high temperatures accelerate sludge breakdown within relatively short retention times (30–60 min), with temperature acting as the primary driver of performance. However, HTTP is energy-intensive and requires specialized infrastructure such as pressurized vessels and automated safety systems, increasing both operational and capital costs [13]. Moreover, temperatures >200 °C can lead to the formation of refractory compounds (e.g., melanoidins) through Maillard reactions, which negatively affect downstream AD performance by inhibiting microbial activity [14,15].

As a result, research has been conducted to evaluate the effectiveness of low-temperature thermal treatments (<100 °C), which are more energy-efficient while still enhancing the hydrolysis of organic matter during AD [16–18]. Combining low-temperature thermal treatment with solar radiation presents a promising strategy to enhance energy efficiency while harnessing renewable energy sources. Although the potential of this strategy has been demonstrated in previous studies using different reactor configurations, solar-assisted thermal pre-treatment remains a novel and underexplored technology [19]. In particular, the use of tubular photoreactors provides the technical solution to merge low-temperature heating with solar energy capture, offering significant potential for pre-treatment applications.

Tubular photoreactors based on compound parabolic collectors (CPC) are designed to capture UV solar radiation with high efficiency, utilizing both direct and diffuse light, a key advantage for solar-driven processes [20,21]. It features a simple yet effective design with two parabolic reflectors that direct solar radiation into the reactor, enhancing light absorption and promoting favourable hydrodynamics, making it scalable for pilot-scale applications [22]. Its non-concentrating design ensures energy-efficient operation under low to moderate solar intensities. Although tubular photoreactors have been extensively applied in water and wastewater treatment, their potential for sludge pre-treatment remains unexplored to the best of our knowledge [21,23–25].

This study investigates a novel pre-treatment strategy combining low temperatures (50, 60, and 70 °C) with solar radiation in a tubular photoreactor to address the dual goals of optimising biogas production and reducing energy inputs. Through this study, the objectives are twofold: 1) to increase methane production through an advanced and sustainable pre-treatment solution for WAS, and 2) to conduct an economic analysis of this technology in a full-scale scenario. Initial tests were performed using a lab-scale CPC photoreactor with simulated solar radiation to optimise operational parameters. Subsequently, the technology was scaled up, and pilot-scale tests were conducted to validate its performance under conditions closer to real-world applications.

2. Materials and methods

2.1. Sources and characteristics of WAS and inoculum

The WAS samples were collected in May 2023 from an urban Wastewater Treatment Plant (WWTP) located on the north of Portugal and stored at 4 °C before use. Its characteristics were as follows: total solids (TS) = 18.1 ± 0.4 g kg^{-1} of sludge, volatile solids (VS) = 15.0 ± 0.1 g kg^{-1} of sludge, total chemical oxygen demand (TCOD) = 21 ± 2 g O_2 L^{-1}, soluble chemical oxygen demand (SCOD) = 128 ± 3 mg O_2 L^{-1}, and pH = 7.3 ± 0.2.

Two trials were conducted for the biochemical methane potential (BMP) tests—one for lab-scale experiments and another for pilot-scale experiments. For both conditions, the anaerobic inoculum consisted of a mixture (50/50, m/m of VS) of anaerobic granular sludge from a brewery treatment plant (Porto, Portugal) and anaerobic digested sludge from WWTP (Braga, Portugal), with a VS content of 13.1 g kg^{-1} and 20.7 g kg^{-1} for the lab-scale and pilot-scale test, respectively.

2.2. Experimental procedure

2.2.1. Tubular photoreactor at lab-scale

The lab-scale system presented in Fig. 1a consists of the following components: (i) a CPC photoreactor unit; (ii) a sunlight simulator (Atlas, model SUNTEST XLS+, Illinois, USA) equipped with a 1700 W air-cooled Xenon lamp (spectral irradiance distribution in Fig. SM-1), a daylight filter and quartz filter with infrared coating, providing 1100 cm^2 of exposition area; (iii) a peristaltic pump (Watson Marlow, 502S model, experimental flow rate set at 96.5 L h^{-1}), to recirculate the WAS between a 1.5 L recirculation vessel and the photoreactor; (iv) a thermostatic bath (Julabo, F12-ED model) for temperature control; (v) a magnetic stirrer (LBX S20 series) to ensure a WAS complete homogenization inside the vessel; (vi) a pH meter; and (vii) a thermometer. All systems are connected by polytetrafluoroethylene (PTFE) tubing with an external diameter of 6 mm.

The sludge temperature within the recirculation vessel was continuously monitored, and the thermostatic bath was adjusted as needed to maintain stable thermal conditions for the WAS throughout the experiments.

The tubular photoreactor comprises a borosilicate glass tube (BT) (Schott Duran type 3.3, Germany) with a cut-off at 280 nm, measuring 200 mm in length, 46.4 mm internal diameter, 1.8 mm thickness, and two polypropylene caps, each one with one inlet/outlet placed in parallel with the fluid flow. The illuminated area is 0.024 m^2. Beneath the BS tube, there is a reflective surface (RS) available in stainless steel tested in three different geometries: (i) simple double parabola (SP); (ii) traditional double parabola (DP), commonly utilized in compound parabolic collectors (CPCs); and (iii) flat (F) (see Fig. 1b). Further details on the dimensions and optical performance of these surfaces are provided by Gomes et al. [26].

For the pre-treatment experiments, 1 L of WAS was introduced into the cylindrical glass vessel and recirculated through the system for 30 min to ensure complete homogenization. For light-assisted experiments, the sunlight simulator was switched on once the desired WAS temperature was reached to initiate the reaction. Hourly samples were collected over a 3-hour period to assess process efficiency by analysing the following parameters: SCOD, temperature, and pH. Solids and TCOD were also quantified for the initial and final samples. Additional analyses were also performed in specific experiments, including characterising extracellular polymeric substances (EPS), volatile fatty acids (VFA), soluble ammonia, rheology, bacterial viability, and BMP tests. At the beginning of each experiment, an initial sample at 25 °C was taken and used as the untreated reference sample (“Control” sample) for comparison purposes. An important factor that influences the comparison between studies is the “heating effect” [19]. This effect corresponds to the degree of disintegration obtained until the desired temperature is reached, which is often neglected. While this could slightly overestimate disintegration, the 25 °C sample was retained as the control to maintain consistency with existing literature, where this effect is often not considered [27,28].

2.2.2. Tubular photoreactor at pilot-scale

The effectiveness of the tubular photoreactor for WAS solubilization was also evaluated using a solar pilot-scale plant (Fig. 2) installed on the Department of Chemical and Biological Engineering rooftop at FEUP

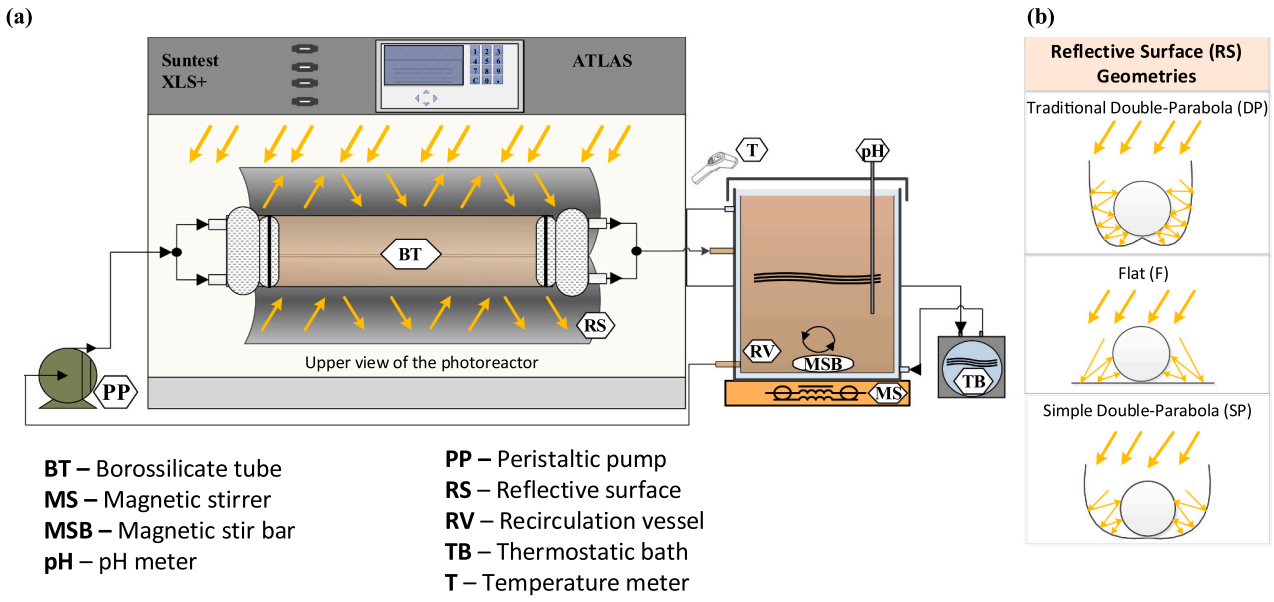


Fig. 1. Schematic representation of the lab-scale tubular photoreactor along with tested reflective surface (RS) geometries.

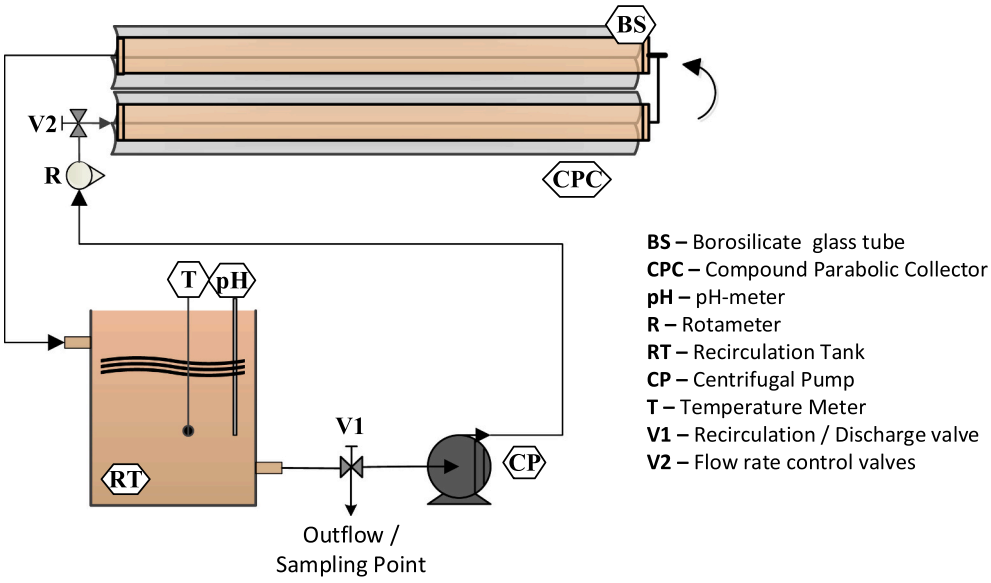


Fig. 2. Schematic representation of the pilot-scale tubular photoreactor.

(Portugal) in August 2023. This setup was oriented southward and tilted at 41° (local latitude) to optimise exposure to natural sunlight.

The pilot-scale plant comprised: (i) two BS glass tubes (Schott-Duran type 3.3, Germany) with a cut-off at 280 nm, measuring 1500 mm in length, 46.4 mm internal diameter, and 1.8 mm thickness, connected in series using polypropylene joints for fluid circulation; (ii) a 20 L recirculation tank equipped with temperature and pH sensors; (iii) a magnetic centrifugal pump for WAS recirculation (Grundfos, model CM5–5 A-R-G-V-AQQV, experimental flow rate set at 1.2 m^3 h^{-1}); and (iv) a rotameter. Each BS glass tube was coupled with an anodised aluminium reflector arranged in a DP geometry, forming a traditional compound parabolic collector (CPC) with a 0.44 m^2 surface area. Data relating to the intensity of natural solar radiation were obtained through the Portuguese Institute for Sea and Atmosphere (IPMA [29]).

Two comparative tests were conducted using the solar pilot-scale unit: (i) a "Sunlight" experiment, with the BS tubes exposed to natural solar radiation; and (ii) a "Dark" experiment, where the BS tubes were covered to block the solar photons. A total of 15 L of WAS was introduced into the system for a 7-hour experiment. An initial sample at 25 °C was the untreated "Control" for comparison. Data points were collected hourly from 9:00 am to 4:00 pm to capture the period of maximum incident radiation. SCOD, temperature, and pH were monitored every hour, with TCOD, solids content, and BMP tests measured at the start and end of each test.

2.2.3. *Experimental design*

The effectiveness of WAS pre-treatment was evaluated under various operating parameters using the lab-scale unit. Initial experiments focused on testing different radiation intensities at a fixed temperature of 60 °C. The sunlight simulator was set to deliver ultraviolet-visible (UV–Vis) irradiances of 375 W m^{-2}, 500 W m^{-2}, and 650 W m^{-2} (spanning the 280–800 nm range), corresponding to ultraviolet (UV) irradiances (280–400 nm) of 41.7, 55.5, and 72.2 W_{UV} m^{-2}, respectively. These values were selected to reflect irradiance levels typically

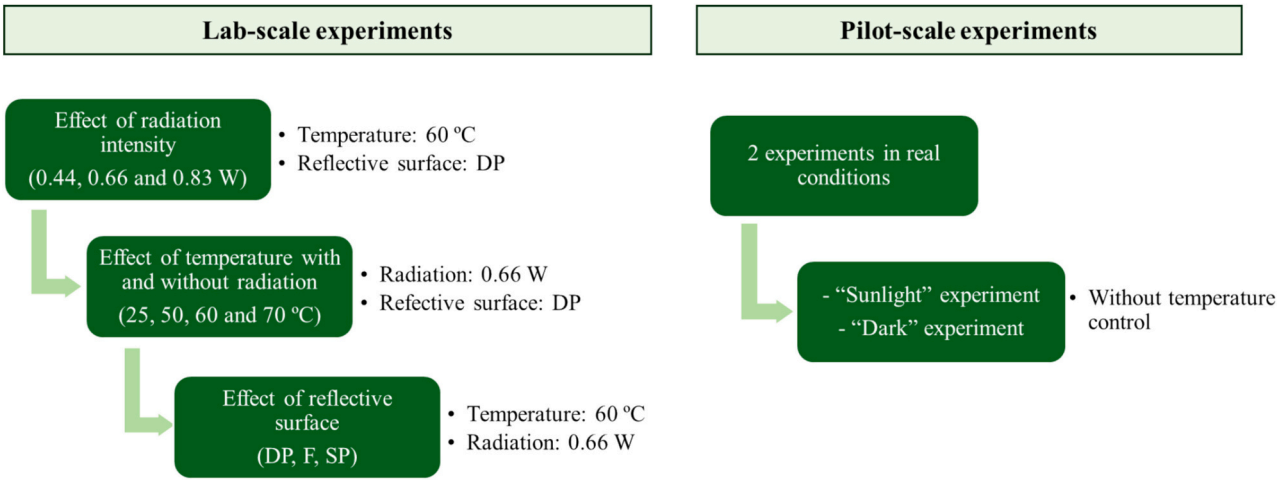


Fig. 3. Experimental stages conducted in this work in the lab-scale and pilot-scale setups.

found in sunny Mediterranean regions under natural solar conditions [19,30]. The actual solar radiant power (RP) reaching the interior of the borosilicate tube was experimentally determined using ferrioxalate actinometry ($[Fe^{3+}] = 6.0 \times 10^{-3}$ M, [oxalic acid] $= 3.0 \times 10^{-2}$ M), as described in [26,31,32]. For each irradiance level tested, the RP values in the UV region (280–400 nm) were 0.45 ± 0.04 W, 0.66 ± 0.04 W, and 0.83 ± 0.05 W, respectively.

Subsequently, WAS pre-treatment was assessed at different temperatures (25 °C set as "Control", 50, 60, and 70 °C) under two conditions: (1) with solar radiation ("Light" experiments), using the selected RP of 0.66 W_{UV}, to assess the combined influence of thermal pre-treatment assisted by solar radiation; and (2) without solar radiation ("Dark" experiments), to isolate the effect of thermal pre-treatment alone. The selected temperature range (50–70 °C) is supported by previous studies demonstrating that mild thermal pre-treatment within this interval can significantly enhance sludge hydrolysis [28,33]. This range also enables assessment of whether the combined application of solar radiation and moderate heat can achieve effective sludge disintegration with reduced thermal energy input, thereby improving the overall energy efficiency and process sustainability.

At the temperature showing promising performance, three reflector geometries were evaluated on WAS solar-thermal pre-treatment, including traditional double-parabola (DP), simple double-parabola (SP), and flat (F) designs.

Finally, after validating the technology performance at lab-scale, two pilot-scale experiments were conducted: one under natural solar exposure and the other in the absence of sunlight ("Sunlight" and "Dark," respectively). A summary of all experimental conditions is provided in Fig. 3 and Table 1.

2.3. Analytical methods

2.3.1. WAS parameters

During the experiments, analyses were conducted to assess both total and soluble fractions of WAS before and after treatment. The supernatant was obtained through centrifugation (4000 rpm/3220 xg for 10 min (CT6E, VWR® Hitachi, USA)) and subsequent filtration (0.45 µm cellulose acetate; Whatman® International) to extract the soluble fraction.

The measurements of TS, VS, total suspended solids (TSS), volatile suspended solids (VSS), and COD (SCOD, TCOD) were conducted according to the procedures described in the Standard Methods for the Examination of Water and Wastewater: 2540B, 2540E, 2540D, 2540E, 5220D, respectively [34]. pH (Edge® Dedicated pH/ORP Meter) and temperature (UNI-T UT300S Infrared Thermometer) were also recorded.

Soluble ammonia was quantified using Hach reagent kits (LCK302; Hach Co., Loveland, Colorado, USA), while VFAs were quantified using high-performance liquid chromatography (Jasco HPLC) (additional details provided in Section 2 of the Supplementary material) for the soluble

Table 1
Operating conditions for WAS pre-treatment trials.

Experiment		Temperature (°C)	Irradiance		RP (W)	Reflector geometry[a]
			($W_{280–800nm}$ m^{-2})	(W_{UV} m^{-2})		
1	Lab-scale	25 ± 1	0	0	0	DP
2			500	55.5	0.66 ± 0.04	
3		50 ± 2	0	0	0	
4			500	55.5	0.66 ± 0.04	
5		60 ± 2	0	0	0	
6			500	55.5	0.66 ± 0.04	
7		70 ± 2	0	0	0	
8			500	55.5	0.66 ± 0.04	
9	Lab-scale	60 ± 2	375	41.7	0.45 ± 0.04	DP
10			650	72.2	0.83 ± 0.05	
11	Lab-scale	60 ± 2	500	55.5	0.54 ± 0.05	F
12					0.64 ± 0.04	SP
13	Pilot-scale	(20–42) ± 2	0	0	0	DP
14		(20–63) ± 2	415[b]	32.5[b]	n.d.	

n.d. - not determined.
[a] DP - traditional double-parabola; SP - simple double-parabola; F – flat.
[b] Values obtained from the data provided by IPMA [29].

fraction.

2.3.2. EPS characterisation

The EPS characterisation focused on carbohydrates (PS) and proteins (PN) across three fractions: soluble EPS (S-EPS), loosely bound EPS (LB-EPS), and tightly bound EPS (TB-EPS). EPS extraction was performed through a sequential centrifugation and heat treatment procedure. Initially, 50 mL of WAS was centrifuged at 10,000 rpm for 15 min to obtain the supernatant as the S-EPS fraction. The resulting pellet was resuspended in a 0.05 % (*w/v*) NaCl solution, heated to 70 °C, vortexed briefly, and centrifuged again to extract the LB-EPS. Subsequently, the remaining pellet was resuspended in fresh NaCl solution and incubated at 60 °C for 30 min, followed by a final centrifugation step to recover the TB-EPS fraction [35]. Protein and polysaccharide concentrations in each fraction were quantified using the modified Lowry method and the phenol–sulphuric acid method, respectively. Further methodological and calibration curve details (Fig. SM-3 and SM-4) are provided in the Supplementary material (Section 3).

2.3.3. Rheology

Shear stress and shear rate were analysed for different WAS samples before and after pre-treatment. The analyses were performed on the total WAS samples using a parallel plate device (PP50) in the range 10^{-3} to 10 s^{-1} of shear rate using a modular compact rheometer model MCR 92 (Anton Paar GmbH). All the analyses were performed in duplicate.

2.3.4. Bacterial viability and faecal coliforms

The membrane integrity of the total fraction of WAS samples, before and after pre-treatment, was assessed using the LIVE/DEAD™ BacLight™ bacterial viability kits (L-7012, Invitrogen Molecular Probes, Massachusetts, USA), according to the manufacturer's protocol [36]. A summary of the procedure is provided in the Supplementary Material. Faecal coliforms were assessed in duplicate following the ISO 4832:2006 after an incubation temperature of 44 °C [37].

2.3.5. Biochemical methane potential assays

BMPs of the total WAS fraction were conducted in 600 mL vessels, following the guidelines established by [38,39]. Each vessel contained 100 mL of working volume, comprising the substrate (WAS), inoculum, and basal medium. The basal medium was prepared by adding 3 g L^{-1} of $NaHCO_3$, macro-and micronutrients, and vitamins, as per Angelidaki et al. [38] (details in Supplementary material). The inoculum was incubated at 37 °C for 5 days to activate microorganisms and deplete the residual substrate [22]. A substrate-to-inoculum ratio of 1:4 (VS basis) was used. Blanks (without substrate) were used to discount the methane resulting from residual substrate present in the inoculum. Control assays using Avicel® (Sigma-Aldrich, St. Louis, MO, USA), a microcrystalline cellulose with an average particle size of 50 μm, were included to evaluate the inoculum quality. All the assays were conducted in triplicate and incubated at 37 °C without light, with regular daily agitation. Methane production was followed by GC analysis. Additional details of the protocol can be found in the Supplementary Material.

2.4. Data processing methods

Accumulated UV energy: The experimental lab-scale results related to the different radiation intensities (Section 3.1) and the different reflective surface geometries (Section 3.3) were plotted in terms of the accumulated UV energy per unit volume (between 280 and 400 nm), as defined by Eq. (1).

$$Q_{UV,n} = \frac{RP \times t_n}{1000 \times V} \quad (1)$$

where Q_{UV} is the accumulated UV energy (kJ L^{-1}) received on the tubular photoreactor, t_n is the time corresponding to *n*-WAS sample (*s*), *RP* is the radiant power (W or J s^{-1}) reaching the interior of the tubular photoreactor, and *V* is the WAS volume (L). The other analytical parameters were plotted against the duration of the experiment (time, in hours).

The Q_{UV} (kJ L^{-1}) received on the pilot-scale unit (Section 3.4) was determined using Eq. (2):

$$Q_{UV,n} = Q_{UV,n-1} + (t_n - t_{n-1})\left(\frac{\overline{I_{UV}} \times A}{1000 \times V}\right) \quad (2)$$

where $\overline{I_{UV}}$ is the average UV irradiance during the time interval $t_n - t_{n-1}$ (W m^{-2}) (source: IPMA [29]), and *A* is the reflective surface area of the CPCs (m^2).

Disintegration degree (DD_{COD}) of the WAS: This metric was used to evaluate the effectiveness of hydrolysis pre-treatment through the analysis of the organic matter solubilization. It measures the transfer of COD from the particulate fraction to the soluble fraction of the WAS during the pre-treatment. DD_{COD} (%) is defined according to Eq. (3), as previously described by [40].

$$DD_{COD} = \frac{SCOD_t - SCOD_0}{TCOD_0 - SCOD_0} \times 100 \quad (3)$$

where $SCOD_t$ is the SCOD of pre-treated WAS (mg O_2 L^{-1}) at *t* hours of pre-treatment, and $SCOD_0$ and $TCOD_0$ are the SCOD and TCOD of initial WAS at 25 °C (mg O_2 L^{-1}).

BMP: defines the maximum amount of methane produced by anaerobic digestion with a specific substrate. It was corrected for standard temperature and pressure (STP) conditions (0 °C and 101.3 kPa) and expressed as the volume of methane at STP conditions per amount of VS of inoculum (L CH_4 kg_{VS}^{-1}) (Eq. (4)) [41].

$$BMP = \frac{V_{CH_4} - V_{CH_{4,blank}}}{VS_{substrate}} \quad (4)$$

where V_{CH4} is the volume of methane (L) produced in the headspace of the bottles, $V_{CH4,\ blank}$ is the volume of methane (L) produced in the blanks, both at STP conditions and VS represents the quantity of VS in the substrate added to each vessel (kg VS) [38]. The controls validated the BMP tests since the criteria (defined in [42]) 352 < BMP < 414 L kg^{-1} VS was fulfilled, as well as the Relative Standard Deviation (RSD) of the triplicates, which was <5 %.

Statistical analyses: To evaluate statistical differences between treatments, the data were first assessed for normality using the Shapiro-Wilk test and for homogeneity of variances with Levene's test. A 2-way ANOVA was then conducted, with radiation and temperature as factors. When necessary, data was ranked to meet the assumptions. The Tukey HSD post-hoc test was applied to the total and fractionation EPS of both PN and PS, except for carbohydrates TB-EPS and DD_{COD} analysis. The Unequal N HSD post-hoc test was used for unbalanced data, such as the BMP. If normality or homogeneity of variances were not met, the non-parametric Mann-Whitney *U* test was performed (particularly for carbohydrates TB-EPS). A balanced *t*-student test assessed differences in SCOD values under various temperatures, both with and without solar radiation. Additionally, bacterial viability was analysed. Significance levels (*p*-values ≤ 0.05, ≤ 0.01, ≤ 0.001, and ≤ 0.0001) are reported in the text, with differences between treatments indicated by letters in the figures. All statistical analyses were conducted using Statistica 7.0.

Microscopic image processing: In the context of image processing, imported microscopic images were handled using the Java-based public domain tool ImageJ, incorporating the RGB measure plugin, in which each image was evaluated considering the green, red, and blue cell percentages.

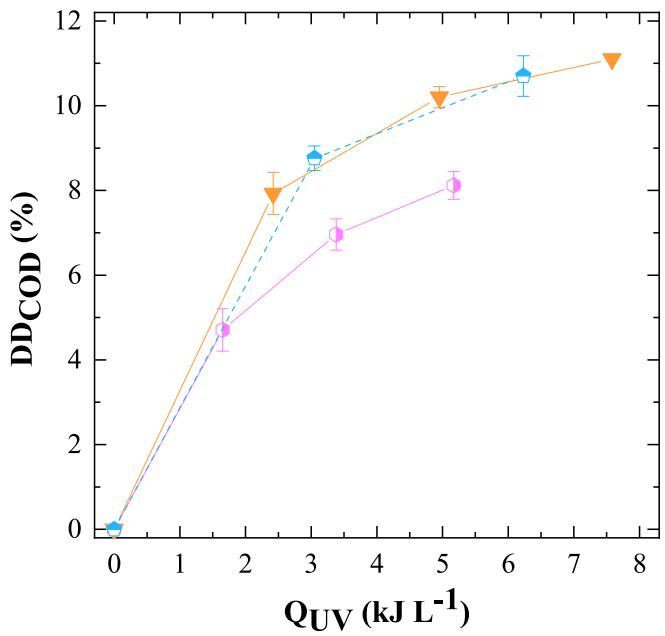


Fig. 4. Disintegration degree (DD_{COD}) as a function of accumulated UV energy (Q_{UV}) during WAS solar-assisted thermal pre-treatment at 60 °C under different RP values (0.45 W_{UV} – ◑; 0.66 W_{UV} – ▼; and 0.83 W_{UV} – ⬟) using DP reflector. Each data point is represented as average values±SD; $n = 2$.

3. Results and discussion

3.1. Impact of radiation intensity on WAS disintegration

The influence of radiation intensity at a constant temperature of 60 °C was investigated by selecting three UV radiant power (RP) values: 0.45 W, 0.66 W, and 0.83 W (Fig. 4, Table SM-1). The outcomes showed similar disintegration rates for RP values of 0.66 W and 0.83 W. In contrast, an RP of 0.45 W resulted in a lower disintegration rate despite the similar accumulated UV energy range.

This observation suggests that an RP of 0.66 W is sufficient to achieve maximum cellular damage, with no additional benefit observed at higher solar radiation intensities (i.e., RP of 0.83 W). In contrast, the lower intensity of 0.45 W was insufficient to induce significant damage, resulting in lower DD_{COD} values (8.1 %). This limited effect may be attributed to the presence of more resistant bacterial populations or aggregates that require higher radiation doses for effective disruption. At this intensity, the radiation likely fails to adequately penetrate or damage these resilient structures, thereby limiting the overall solubilization efficiency [42]. The higher DD_{COD} values, attributed to solar radiation's disintegration effect, are driven by the bactericidal properties of ultraviolet A (UVA, 315–400 nm) and B (UVB, 280–315 nm) radiation, which damage cell membranes and induce cell death [43]. UVB radiation directly affects microbial cells by generating reactive oxygen species (ROS), leading to oxidative stress and disrupting DNA replication, causing DNA mutations and cell death [44]. In addition, solar UVB exposure—particularly within the temperature range of 30–60 °C—can further suppress catalase activity, weakening the cell's protection against oxidative stress and allowing ROS, including oxidants as H_2O_2, to accumulate more freely [45,46]. These ROS possess strong antimicrobial properties and can severely damage bacterial cells by interacting with membrane lipids—altering their assembly, composition, structure, and dynamics. Such disruptions compromise membrane integrity, contributing to cell lysis and enhanced WAS disintegration [47,48]. Other relevant mechanisms include: i) internal Fenton; ii) external photo-Fenton reaction, in which UV radiation facilitates the reaction between iron ions (Fe^{2+}/Fe^{3+}) and hydrogen peroxide (H_2O_2), generating hydroxyl radicals ($HO^{\bullet}$) [44]. These radicals further intensify oxidative damage and promote microbial cell breakdown.

Although ROS generation is a plausible mechanism underlying these effects, direct quantification of ROS in complex matrices like WAS remains challenging due to the heterogeneous nature of the sludge and the short-lived nature of ROS species [49]. As a result, the present study focused on evaluating the overall disintegration effects induced by different radiation intensities, rather than quantifying ROS or delineating specific mechanistic pathways. Nevertheless, the observed improvements in solubilization and microbial disruption are consistent with ROS-mediated effects reported in the literature. When both UVA and UVB are present during simulated solar exposure, the resulting DNA damage typically resembles that caused by UVB radiation [50]. Given that the solar simulator spectrum used in this study was dominated by UVA radiation, with lower UVB contribution, the indirect oxidative mechanisms are expected to predominate (Fig. SM-1).

3.2. Impact of temperature on the WAS disintegration

After selecting an RP of 0.66 W for subsequent experiments, a comprehensive analysis of the isolated effect of temperature and the combined effects of temperature and solar radiation was conducted over a 3-hour period (Fig. 5a, Table SM-1). This duration was sufficient to achieve stable SCOD values for all the tested conditions, consistent with previous works, which have shown that the most substantial rise in SCOD occurred within the initial 3 h of the process [16,28]. A kinetic model, proposed by Liew et al. [28], was fitted to the experimental data displayed in Fig. 5a to describe the solubilization of organic matter during WAS hydrolysis. This model assumes that the hydrolysis process follows first-order reaction kinetics, where the conversion rate of particulate compounds into soluble ones is proportional to the concentration of the remaining particulate substrate. Particularly, it quantifies the accumulation of SCOD over time as a function of the particulate chemical oxygen demand (PCOD), as shown in Eq. (5):

$$SCOD = SCOD_0 + \alpha PCOD_0\left(1 - e^{-kt}\right) \quad (5)$$

where α corresponds to the conversion coefficient of the substrate to product (g SCOD g^{-1} PCOD), PCOD represents the particulate COD (mg O_2 L^{-1}), calculated according to Eq. (6), k is the first-order rate constant (h^{-1}) and t the duration of the trial (h).

$$PCOD_0 = TCOD_0 - SCOD_0 \quad (6)$$

In this model, PCOD was used as a proxy for VSS, due to the strong correlation between these parameters in sewage sludge. The kinetic parameters k and α were estimated by nonlinear regression using Microsoft Excel Solver, by minimising the sum of squared errors between experimental and predicted SCOD values.

The k ranged between 0.02 ± 0.01 h^{-1} and 2.0 ± 0.2 h^{-1}, with a good fit between the model and the experimental data (see Table 2). These k values were higher than those typically reported in studies of mild-temperature pre-treatments of WAS from urban WWTPs, where values usually fall between 0.05 and 0.80 h^{-1} [28,51].

The tested pre-treatments demonstrated a consistent trend: increasing temperature and extending treatment duration improved COD solubilization compared to the control WAS sample (25 °C) (Fig. 5a). The highest efficiency was obtained at 70 °C under solar radiation, resulting in a 9.1-fold SCOD concentration increase relative to the "Control" (p-value ≤0.001) after 3 h. Higher temperatures (60 °C and 70 °C) enhanced COD solubilization, which is consistent with previous studies indicating high enzymatic activity within 60 °C and 75 °C [19,28,52]. The SCOD increase also indicates that more complex organic compounds were converted to soluble monomers and that microbial cells were disrupted, leading to cell lysis during pre-treatment [53,54]. The release of organic matter caused by WAS floc disintegration and microbial cell lysis was assessed by the variations in SCOD through the

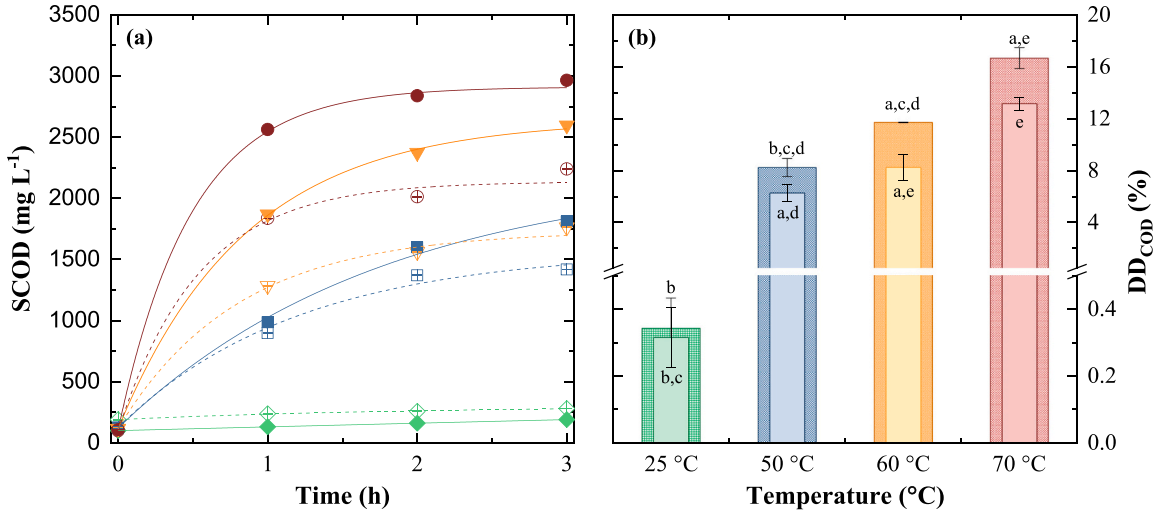


Fig. 5. Effect of pre-treatment temperature (25 °C – ◆◇; 50 °C – ■□; 60 °C – ▼▽; 70 °C – ●○) on WAS hydrolysis, under simulated sunlight (solid symbols and patterned bars; RP = 0.66 W_{UV}) and dark conditions (open symbols and solid bars): (a) evolution of soluble chemical oxygen demand (SCOD) over time with corresponding fitting curves; and (b) representation of disintegration degree (DD_{COD}) as a function of temperature. Data are presented as average values±SD ($n = 2$); superscript letters indicate significant differences (Tukey HSD test, p-value ≤0.05) between experiments (see Table SM-2).

Table 2
First-order kinetic coefficients (k) for WAS hydrolysis at different pre-treatment temperatures (25, 50, 60 and 70 °C) under simulated sunlight and dark conditions (here represented as "Light" and "Dark", respectively). Each point was represented by average values±SD; $n = 2$.

Experiment	α[a] (g SCOD g^{-1} PCOD)	k (h^{-1})	R^2[b]	Sr^2[c] (mg O_2 L^{-1})^2
25 °C, Dark	0.0650 ± 0.0004	0.02 ± 0.01	0.999	0.02
25 °C, Light	0.0051 ± 0.0008	0.5 ± 0.1	0.992	1.6
50 °C, Dark	0.067 ± 0.006	0.8 ± 0.2	0.992	310
50 °C, Light	0.103 ± 0.009	0.6 ± 0.1	0.996	137
60 °C, Dark	0.077 ± 0.003	1.3 ± 0.1	0.990	154
60 °C, Light	0.114 ± 0.002	1.2 ± 0.1	0.999	64
70 °C, Dark	0.115 ± 0.005	1.9 ± 0.4	0.990	332
70 °C, Light	0.140 ± 0.002	2.0 ± 0.2	0.999	117

[a] α means the substrate conversion.
[b] R^2 is the coefficient of determination.
[c] Sr^2 is the residual variance.

disintegration degree (DD_{COD}) [55]. Across all investigated pre-treatment temperatures, a significant enhancement in COD solubilization (SCOD) was recorded (p-value ≤0.05), resulting in a 6 to 17 % DD_{COD} increase compared to "Control" (Fig. 5b, Table SM-1). The present findings align with previous studies of low-thermal pre-treatment, where DD_{COD} results ranged between 1 and 25 % [16,28,56,57]. This range of DD_{COD} values can be due to the diverse origins of WAS and its inherent differences, making direct comparisons of SCOD values and disintegration rates challenging. For instance, Ruffino et al. [16] reported a DD_{COD} of 20.2 % after a low-thermal pre-treatment at 70 °C for 3 h. In contrast, the present work achieved a DD_{COD} of 11.8 % under similar thermal conditions. However, with the addition of solar radiation at 70 °C, the DD_{COD} reached 17 %, highlighting the significant contribution of solar radiation in enhancing disintegration efficiency.

The results indicate that solar radiation enhances DD_{COD} by approximately 4 % at each tested temperature, demonstrating its positive impact on optimising pre-treatment strategies. However, temperature remains the most significant factor with an impact on WAS disintegration (p-value ≤0.001), as it provides the kinetic energy necessary to break the chemical bonds within biopolymers [28]. High temperatures also cause the denaturation or reduction of biomolecules with high water affinity, such as proteins, carbohydrates, and nucleic acids, which alters the sludge matrix composition [58,59].

Various pre-treatment technologies have been explored in the literature to improve sludge disintegration prior to AD. For instance, thermo-chemical methods using alkaline agents (e.g., NaOH) or oxidants (e.g., H_2O_2) can achieve DD_{COD} values ranging from 16 % to 29 % at temperatures between 60 and 70 °C within 30 to 60 min of treatment [45,57]. Acid pre-treatments have shown similarly broad DD_{COD} ranges, varying from 8.5 % to 27.8 %, while alkaline treatments range between 1.8 % and 26.9 %, depending on dosage, temperature, and sludge characteristics [60]. While effective, these methods increase operational costs and carry environmental concerns related to reagent handling and potential formation of inhibitory by-products. Ultrasonic pre-treatments also show variable performance: DD_{COD} values ranging from 6 % to 30 % have been reported under conditions such as 0.5 W mL^{-1} with 20 to 80 min of sonication at 20 kHz, whereas significantly lower efficiencies (e.g., 2.5 %) have been observed under other conditions (1 W mL^{-1}, 15 min) [61,62]. Despite their effectiveness in some cases, these approaches demand high energy input and complex equipment, limiting their practical scalability. Biological pre-treatments, including fungal or enzymatic strategies, are environmentally friendly and operate under ambient conditions. However, they often require extended retention times (24–72 h) and yield variable disintegration efficiencies—typically in the range of 5–15 % DD_{COD}—due to microbial sensitivity and system instability [60]. Moreover, discrepancies in reported pretreatment efficiencies across studies are frequently attributed to differences in sludge composition and operating conditions during thermal hydrolysis or other processes [63].

3.2.1. *Pre-treatment effect on the microbial cells structure*

The WAS is composed of diverse microbial cell structures, such as EPS, cell walls, membranes, and cell nuclei [64]. The SCOD increase suggests microbial damage during low thermal pre-treatment, leading to the release of soluble materials. Therefore, EPS modification, VFAs, ammonia, rheology, cell lysis, and faecal coliforms were assessed to evaluate thermal pre-treatment effects.

3.2.1.1. EPS. EPS play a crucial role in enhancing the sludge's water-binding capacity as it adheres to the surface of microbial cells and flocs [65]. These substances are primarily composed of carbohydrates (PS, ca. 11 %) and proteins (PN, ca. 61 %), with smaller amounts of lipids, humic substances, nucleic acids, and other unidentified compounds [53,66]. S-EPS (Fig. 6) reflects the extent of PN and PS

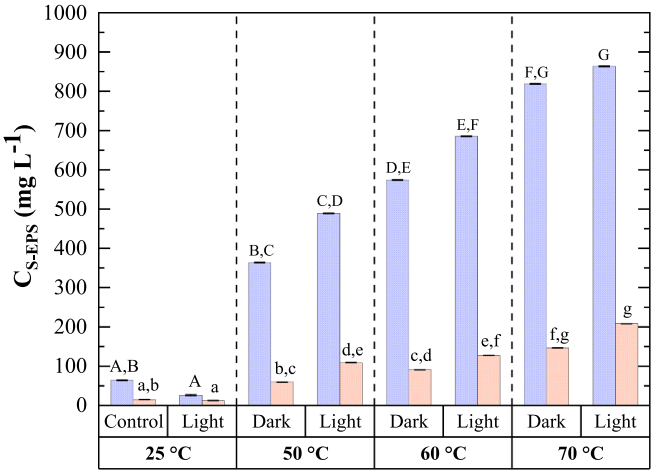


Fig. 6. Concentration of soluble extracellular polymeric substances (S-EPS) represented as proteins (PN, ▭) and carbohydrates (PS, ▭) during 3-hour WAS pre-treatment at different temperatures under "Light" (RP = 0.66 W_{UV}, equivalent to 7.6 kJ_{UV} L_{WAS}^{-1}) and "Dark" conditions. Bars represent average values±SD; $n = 2$; superscript letters denote significant differences in PN (uppercase letters) and PS (lowercase letters) concentrations, according to Tukey HSD test, p-value ≤0.05 (see Tables SM-3.1 to SM-3.5).

solubilization, which is a key indicator of pre-treatment efficiency in breaking down the sludge matrix.

PN and PS concentrations were significantly influenced by the pre-treatment conditions when compared to the "Control" (p-value ≤0.001). An increase in temperature to 70 °C, combined with UV radiation, led to a significant rise in S-EPS concentration (p-value ≤0.001), showing a ca. 14-fold increase in PN (from 64 to 864 mg L^{-1}) and PS (from 15 to 208 mg L^{-1}) compared to the "Control".

Incorporating solar radiation into the WAS pre-treatment process further enhanced PN and PS solubilization (p-value ≤0.01), achieving up to a 1.8-fold increase. These observations align with previous studies, highlighting that UVB radiation can induce damage in proteins and other complex structures [50,67].

An antagonist profile was observed between the LB-EPS and TB-EPS fractions: as LB-EPS increased, TB-EPS decreased (Fig. 7a and b). This redistribution of substances from the inner to the outer layers of the EPS indicates potential membrane rupture, weakening the binding of EPS to the sludge flocs [28]. Additionally, the absolute content of PN was higher than PS, reflecting that proteins constitute more than half of the organic substances in microorganisms [68].

Higher temperatures were more effective in releasing the TB-EPS from WAS, with significant differences (p-value ≤0.05) observed in experiments at 50 °C with radiation and at 60 °C and 70 °C with and without radiation, compared to the "Control". Since experiments were conducted at temperatures between 50 °C and 70 °C, PS solubilization was slightly lower than PN solubilization, with a difference of approximately 0.5 to 1-fold. These results suggest a synergistic mechanism between thermal stress and solar radiation. Elevated temperatures destabilise cell membranes and weaken the EPS matrix, while UV-induced photochemical reactions generate ROS that further damage microbial cells and denature proteins and carbohydrates [12,69]. This combined effect likely promotes the release of TB-EPS into more soluble fractions (LB-EPS and S-EPS), accelerating EPS solubilization efficiency.

It is also important to note that certain EPS components, particularly polysaccharides, are more resistant to thermal degradation and typically require temperatures above 75 °C for effective depolymerization [28]. This difference can be attributed to the distinct origins and thermal sensitivity of these compounds. Proteins originate from both EPS and intracellular sources released through cell lysis, which occurs at moderate temperatures, making PN more readily solubilised under the tested conditions [27,70]. In contrast, polysaccharides are primarily located in EPS exopolymers, which are more resistant and require higher temperatures for effective solubilization.

3.2.1.2. Changes in ammonia and VFAs content. The decomposition of nitrogen-containing organics, mainly derived from the breakdown of proteins during pre-treatment, results in the release of ammonia (NH_4^+-N) (Fig. SM-5) [71]. Ammonia concentrations remained relatively stable across different pre-treatments, reaching a maximum of 158.2 mg L^{-1} of NH_4^+-N at 60 °C (dark mode), with a slight reduction at 70 °C, possibly due to volatilization [70]. However, none of them reached free ammonia concentrations above 900 mg L^{-1} of NH_4^+-N, which are known to inhibit mesophilic anaerobic digestion and adversely affect the microbial community, particularly methanogens, which are crucial for biogas production [72–74].

The pre-treatment resulted in similar VFAs concentrations (2 g_{COD} L^{-1}) when compared to the "Control" (nearly 0 g_{COD} L^{-1}), primarily due to the disintegration of biological cells, macromolecules, and proteins, which can also promote acidogenesis and VFAs production [75,76]. This

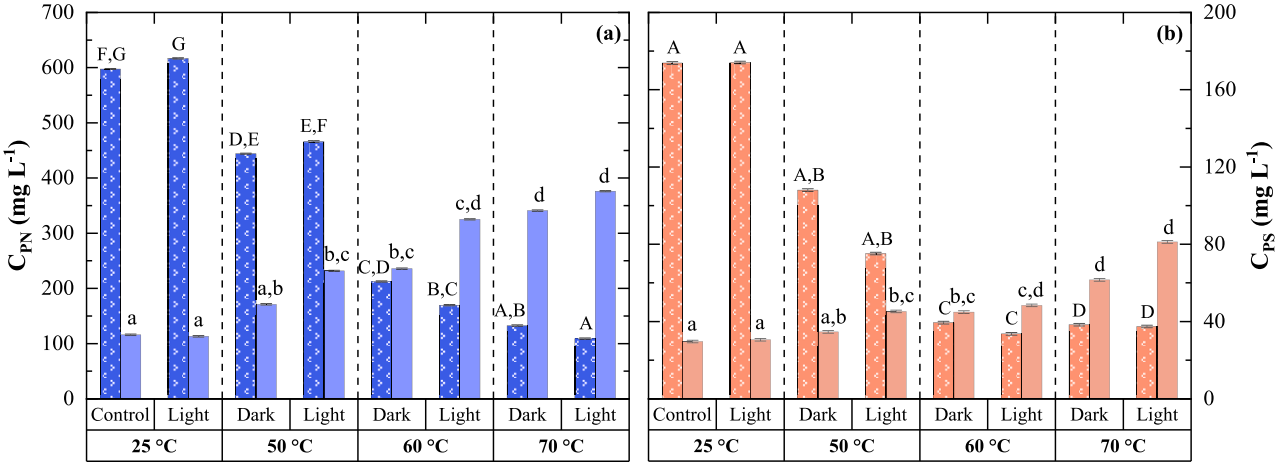


Fig. 7. Concentration of loosely bound EPS (LB-EPS – solid bars) and tightly bound EPS (TB-EPS – patterned bars) for (a) proteins (PN) and (b) carbohydrates (PS) during 3-hour WAS pre-treatment at different temperatures under "Light" (RP = 0.66 W_{UV}, equivalent to 7.6 kJ_{UV} L_{WAS}^{-1}) and "Dark" conditions. Bars represent average values±SD; $n = 2$. Significant differences (parametric Tukey HSD, p-value ≤0.05) among treatments are represented as superscript letters, with uppercase and lowercase letters used for the TB-EPS and LB-EPS fractions, respectively. Significant differences in the TB-EPS fraction of PS across temperatures were identified using the Kruskal-Wallis test.

increase was accompanied by a decrease in pH, from 7.3 to 6.9, likely linked to VFA accumulation, important intermediates in the anaerobic digestion process (Fig. SM-5) [57].

3.2.1.3. Rheology. Visually, the pre-treated WAS appeared less viscous, exhibiting improved fluid recirculation throughout the system. These visual observations were corroborated by rheological tests, which demonstrated a decrease in apparent viscosity for all pre-treated samples compared to the "Control" sample (Fig. SM-6).

Solar radiation did not impact viscosity behaviour, as similar performances were observed with and without radiation at the same temperatures. This reduction in apparent viscosity with temperature

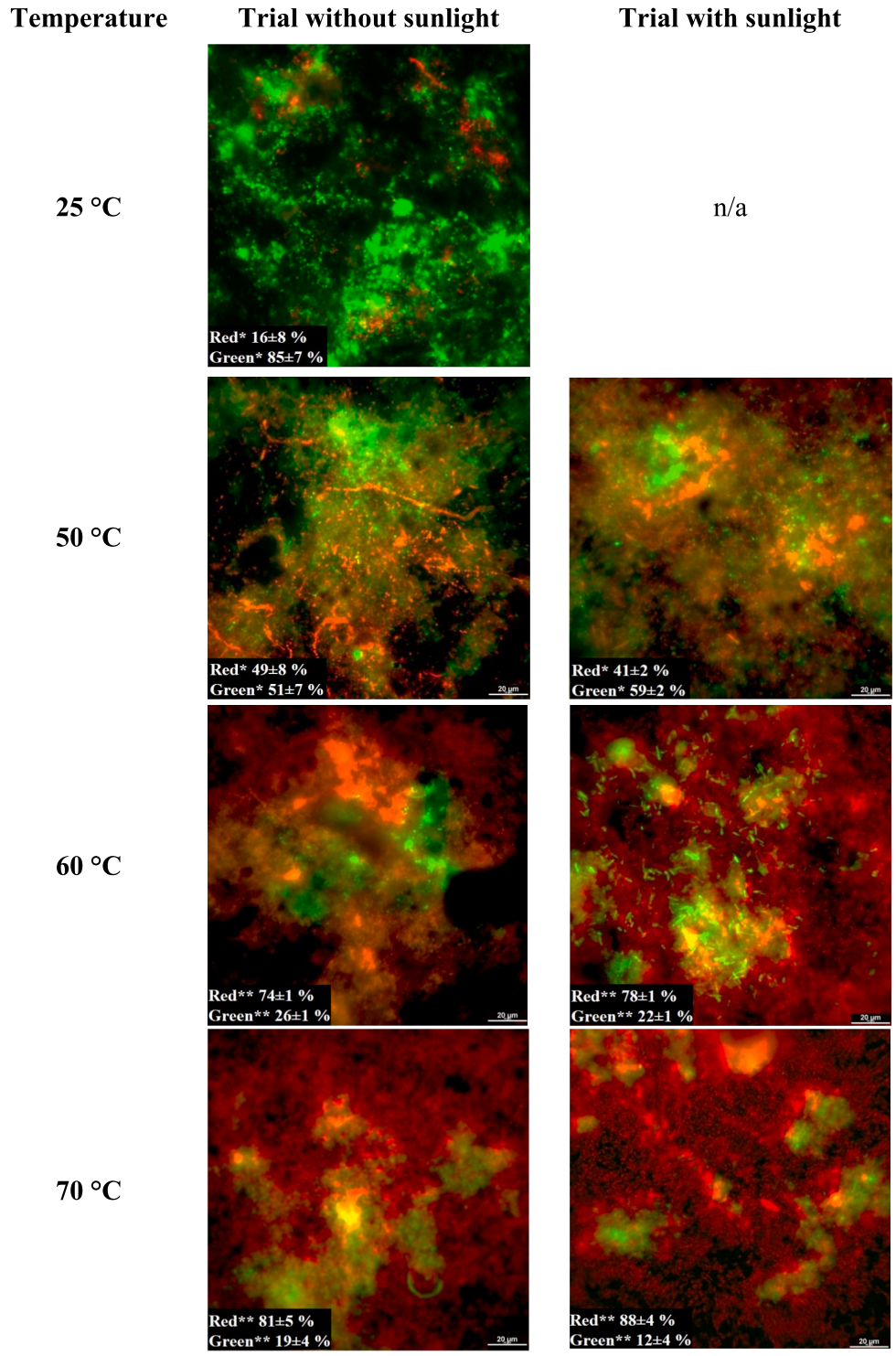


Fig. 8. Microscopic images obtained using the LIVE/DEAD™ BacLight™ viability assay for the control sample (25 °C, without sunlight) and WAS samples after 3-hour pre-treatment at different temperatures in the absence and presence of sunlight (RP = 0.66 W_{UV}, equivalent to 7.6 kJ_{UV} L_{WAS}^{-1}). Viable cells appeared with green fluorescence, while dead cells exhibited red fluorescence, with their respective percentages displayed in the bottom-left corner of each image. Due to its negligible contribution, the sample subjected to solar radiation at 25 °C was not analysed (n/a). Significant differences (t-student test, * for *p*-value ≤0.05, ** for p-value ≤0.001) were performed against the "Control" group. Data are presented as average values±SD; $n = 2$.

increase is consistent with the literature [77–79]. According to Farno et al. [78], this decrease in apparent viscosity is influenced by both temperature and heating duration, with the latter critical at lower temperatures and lower shear rates. In this study, a more pronounced difference in apparent viscosity was observed at lower shear rates (Fig. SM-6), where the structural integrity and chemical forces within sludge macromolecules dominate, as described by Ruffino et al. [16]. The observed reduction in viscosity can be attributed to increased organic matter solubilization following pre-treatment, which includes the solubilization of EPS. This process releases bound water content and disrupts the initial structure of the sludge flocs [80,81]. Thus, the pre-treatment processes weakened the non-Newtonian characteristics of the sludge, further decreasing the apparent viscosity [82]. This enhancement could facilitate better fluid mixing and pumping within the system, thereby improving mass transfer rates, reducing dead zones, and ultimately enhancing process efficiency and cost-effectiveness [16,83,84].

3.2.1.4. Microbial integrity and hygienisation of WAS. Evaluating bacterial damage in WAS before and after pre-treatments, under varying temperatures with and without solar radiation, is critical for assessing treatment effectiveness (results shown in Fig. 8). This analysis provides insights into the effectiveness of the methods in inactivating bacteria, which is essential for ensuring the efficiency of subsequent steps.

The pre-treated samples showed a significantly (p-value $\leq$0.05) higher proportion of non-viable cells (over 45 % dead bacteria) with increasing temperature compared to the "Control", which had more than 80 % of viable cells [85]. The temperature increase resulted in a more significant proportion of non-viable cells (p-value $\leq$0.05). In contrast, the additional effect of solar radiation on non-viable cells was not statistically significant (p-value >0.05). This suggests that temperature was the dominant factor in causing cell membrane disruption and lysis, leading to the release of intracellular contents and increased SCOD and S-EPS (as discussed in Sections 3.2 and 3.2.1.1). Nevertheless, the contribution of solar radiation cannot be disregarded. Although not statistically dominant, UV exposure likely intensified cellular stress and weakened membrane integrity through oxidative and photochemical effects [69]. This additional stress may have facilitated the release of intracellular contents, thereby enhancing solubilization processes and contributing to increased microbial cell death.

It is also known that minimising pathogenic microorganisms in sludge is crucial to prevent surface and groundwater contamination [86]. Faecal coliform analysis of untreated WAS displayed a count of 1.3×10^5 ufc g^{-1} exceeding the threshold of 1×10^3 ufc g^{-1} for Class A sludges according to the EPA U.S. 40 CFR Part 503 [87]. After all case studies pre-treatments, a noticeable reduction in faecal coliform count was observed, bringing levels below the detection limit (DL, 1.0×10^1 ufc g^{-1}). Faecal coliforms can survive at mesophilic temperatures (i.e., up to 45 °C) [88,89]; however, temperatures above 45 °C significantly reduce pathogen levels, as demonstrated by Bonjoch and Blanch [86]. Consistent with these findings, this study effectively reduced pathogenic bacteria in WAS to undetectable levels, resulting in sanitized sludge [87].

3.2.2. Methane production after WAS pre-treatment

The BMP test showed that all pre-treated samples achieved significantly higher methane yields compared to the "Control" (*p*-value $\leq$0.05, Fig. 9, Table SM-1), with specific methane production increasing from 156 ± 10 L CH_4 kg_{VS}^{-1} to 212 ± 6 L CH_4 kg_{VS}^{-1} as the temperature raised from 50 °C (without radiation) to 70 °C (with solar radiation). This corresponds to at least a 1.3-fold increase compared to the "Control" group (118 ± 8 L CH_4 kg_{VS}^{-1}), demonstrating that the thermal pre-treatment effectively enhanced WAS disintegration without causing inhibition in a downstream anaerobic digestion process. The absence of a lag phase in methane production, with peak levels observed between

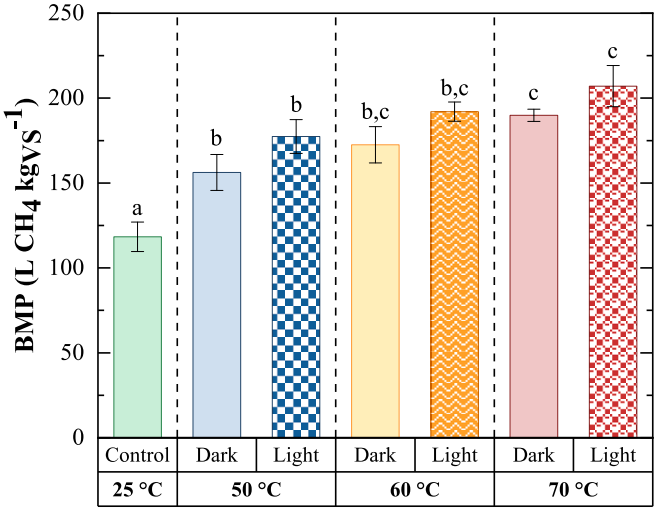


Fig. 9. Methane yield from the 31-day biochemical methane potential (BMP) test for the "Control" sample (at 25 °C) and WAS samples pre-treated for 3 h at different temperatures under simulated sunlight (patterned bars; RP = 0.66 W_{UV}, equivalent to 7.6 kJ_{UV} L_{WAS}^{-1}) and dark conditions (solid bars). Bars represent average values±SD; n = 3; superscript letters indicate significant differences between the "Control" and the different experiments (Unequal N HSD post-hoc test, *p*-value $\leq$0.001).

days 26 and 31 (Fig. SM-7), further supports this conclusion [65].

At the same temperature, methane yield increased by approximately 11 % when solar radiation was applied compared to conditions without it. Notably, methane production at 50 °C with sunlight was similar to that at 60 °C in the dark (p-value >0.05). A similar trend was observed at 60 °C with solar irradiation compared to 70 °C in the dark (*p*-value >0.05). These results underscore the energy-saving potential of incorporating solar radiation into the thermal pre-treatment process, enabling comparable methane production at temperatures up to 10 °C lower. Although the 70 °C pre-treatment demonstrated the highest COD solubilization and resulted in the highest methane production yields, increasing the temperature from 60 °C to 70 °C may be unnecessary, given the energy-efficient results obtained at 60 °C with solar radiation. Therefore, 60 °C was selected for further investigation, as it offers a practical balance between process efficiency, cost-effectiveness, maintenance, and feasibility for lab-scale testing.

3.3. Impact of reflective surfaces on WAS disintegration

The degree of WAS disintegration was compared for three reflective surface geometries – flat (F; RP = 0.54 ± 0.05 W_{UV}), simple double parabola (SP; RP = 0.64 ± 0.04 W_{UV}), and double parabola (DP; RP = 0.66 ± 0.04 W_{UV}) – to evaluate their effect on the performance of the solar-assisted thermal pre-treatment at a controlled temperature of 60 °C (Fig. SM-8, Table SM-1). Results revealed no significant difference in disintegration rates across the various reflective surface geometries (p-value >0.05), consistent with the minor variations observed in the RP provided by each geometry. Accordingly, the accumulated UV energy within the reactor after 3 h of sunlight exposure remained similar across the different surface geometries at ca. 7 kJ_{UV} L^{-1}.

The flat geometry is recognized for its simplicity, cost-effectiveness, and efficiency in minimising the distance between absorber tubes. As noted by Gomes et al. [26] and Silva et al. [75], who studied the impact of different solar collectors on the treatment of landfill leachate and antibiotic-contaminated water via photo-Fenton reaction and heterogenous photocatalysis, where solar thermal energy concentration is not a primary concern, flat reflectors can be advantageous in certain applications. However, the WAS thermal pre-treatment at the pilot-scale unit (Section 3.4) employed the DP geometry. This choice was influenced by

the higher viscosity of WAS compared to other liquid streams, making the DP design more suitable for optimising energy capture in tubular photoreactors. The DP geometry, a widely adopted and proven option for scale-up, excels in concentrating both direct and diffuse solar radiation, thereby enhancing thermal performance [90]. In this way, despite the advantages of the flat geometry in some contexts, the DP configuration remains the preferred option for maximising energy efficiency in solar concentrators at the pilot scale.

3.4. Evaluation of WAS disintegration at pilot-scale

Following the lab-scale testing conducted at controlled temperatures using an external heating source, two outdoor pilot-scale experiments were carried out during a 7-hour period in the summer season within a CPC-based tubular photoreactor without active heating (Fig. 10, Table SM-1): (i) one under natural solar radiation ("Sunlight"); and (ii) another in the absence of sunlight ("Dark"), where an opaque material covered the reaction structure to block solar UV–Vis photons. In the "Sunlight" experiment, solar UV irradiance (I_{UV}) reached its peak of ca. 44 W_{UV} m^{-2} around midday (1 pm), 4 h after the experiment began. This resulted in a consistent accumulation of UV energy on the tubular photoreactor, reaching 16.6 kJ_{UV} L^{-1} by the 4-hour mark (Fig. 10a.1). Over the subsequent 3 h, an additional 12.1 kJ_{UV} L^{-1} was accumulated, bringing the total UV energy to 28.7 kJ_{UV} L^{-1} by the end of the experiment.

During the first 4 h of the "Sunlight" experiment (16.6 kJ_{UV} L^{-1}), the WAS temperature gradually increased from 20 to 62 °C, achieving a DD_{COD} of 6.9 % (Fig. 10a.2), entirely through self-heating driven by natural sunlight exposure. This demonstrates the potential for solar energy to autonomously reach the required pre-treatment temperatures and enhance WAS disintegration without reliance on external heating devices. Notably, in the final 3 h (12.1 kJ_{UV} L^{-1}), the temperature stabilized around 63 °C, achieving a DD_{COD} of ca. 12 %, comparable to the values observed at lab-scale experiments conducted at 60 °C with radiation (i.e. 11 %). These results suggest that the proposed solar-assisted setup could be a viable and sustainable alternative for real-scale implementation. However, it is important to acknowledge that these results reflect the specific conditions of the summer season (August 2023), and seasonal variations may influence the outcomes. In contrast, under "Dark" conditions, where the temperature did not reach even 45 °C, the DD_{COD} was only 1 %, suggesting a minimal release of organic compounds. These findings are consistent with Prorot et al. [18], who concluded that WAS disintegration occurs only at temperatures above 50 °C, further supporting the temperature threshold required for effective disintegration, which only occurred in combination with solar radiation.

Despite the absence of a statistically significant difference (p-value >0.05) between the sample pre-treated in the "Dark" experiment and the "Control" sample, methane production under the "Dark" condition was 35.8 % higher. This increase is likely due to the temperature rise from 20 to 42 °C observed during the "Dark" experiment, which can be attributed to infrared (IR) radiation absorption. Solar IR photons can be absorbed by the covering material and converted into thermal energy, potentially contributing to the enhancement of methane production [91,92]. Remarkably, the WAS sample pre-treated in the "Sunlight" experiment attained 84.9 % higher (206 vs. 112 L CH_4 kg_{VS}^{-1}) methane production compared to the "Control" sample (p-value ≤0.001) and 36.1 % higher (206 vs. 151 L CH_4 kg_{VS}^{-1}) than the "Dark" sample (p-value ≤0.05), highlighting the effectiveness of solar radiation in boosting methane production yields (Fig. 10b). Extrapolating these results to a real-scale WWTP processing 36,000 m^3 of WAS annually, with an average VS concentration of 33 g L^{-1}, the additional methane production is 111,672 m^3, leading to a total methane yield of 244,728 m^3 after pre-treatment (calculated using Eq. SM-1).

In summary, these findings reinforce the significant influence of solar radiation on WAS thermal pre-treatment, facilitating temperature elevation and subsequent enhancement in the disintegration degree of the sludge, which supports the results presented in Section 3.2 regarding the effect of solar radiation. This, in turn, accelerates the hydrolysis rate, resulting in a notable improvement in methane production.

3.5. Scale-up and economic assessment

This section evaluates the economic feasibility of scaling up the

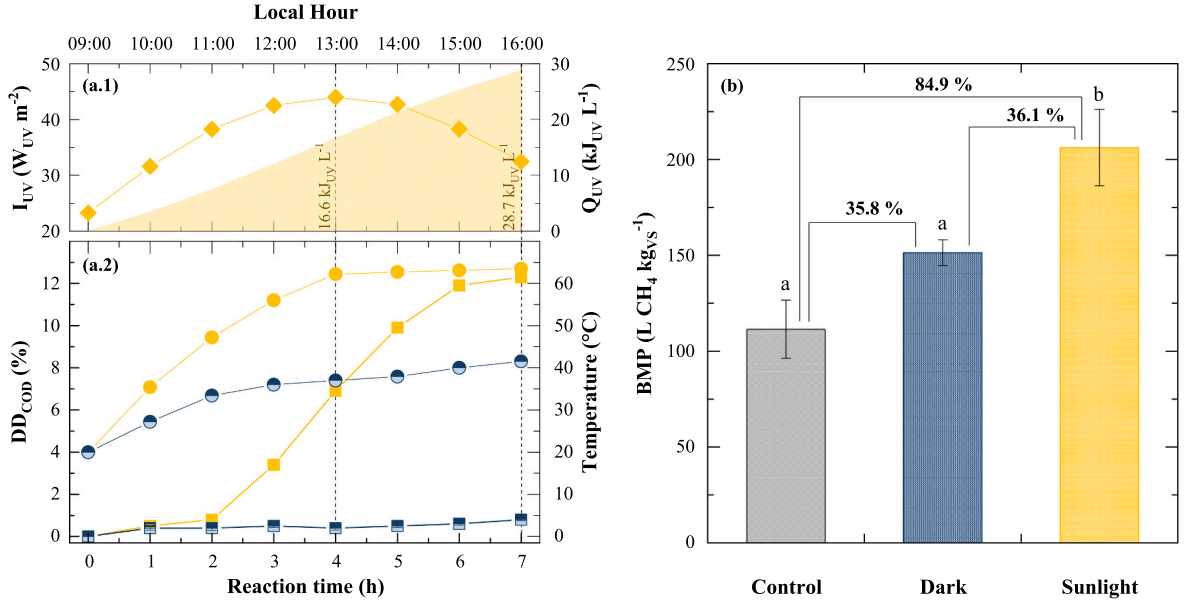


Fig. 10. Pilot-scale WAS thermal pre-treatment under natural sunlight (solid symbols and shaded area) and dark conditions (semi-filled symbols) conducted on 7th and 9th August 2023, respectively: (a) temporal profile of (a.1) solar UV irradiance (I_{UV} – ◆) along with accumulated UV energy (Q_{UV} – ▭) and (a.2) disintegration degree (DD_{COD} – ■◨) along with temperature (●◓); and (b) methane yields from 27-day biochemical methane potential (BMP) tests for control sample and pre-treated samples. Each symbol/bar represents average values±SD, with n = 2/3; statistical comparisons between treatments were performed using the Unequal N HSD post-hoc test.

proposed CPC-based tubular photoreactor for WAS solar-assisted thermal pre-treatment, targeting an 84.9 % increase in the methane production (from 111 to 206 L CH_4 kg_{VS}^{-1}, Fig. 10b) during the subsequent anaerobic digestion process, as achieved in the pilot-scale experiments under natural sunlight. In addition to methane production, the scale-up and cost analyses were based on the accumulated UV energy (Q_{UV}) observed during the pilot-scale "Sunlight" experiment, considering two scenarios:

- Scenario 1 (without external heating): Assumes the entire pre-treatment process relies solely on natural solar radiation to provide the necessary UV photons and induce any required WAS self-heating. In this case, the Q_{UV} of 28.7 kJ_{UV} L^{-1} was calculated over the whole 7-hour pilot-scale experimental period (see Fig. 10a.1).
- Scenario 2 (with external heating): Assumes an external heat source is integrated into the CPC unit to pre-heat the WAS to the target temperature (60 °C) before initiating the solar-driven treatment while also supplementing solar thermal energy during the process if necessary. The objective is to analyse whether this approach can improve the system's performance by minimising the overall solar energy demand and the required CPC area. In this setup, the Q_{UV} of 12.1 kJ_{UV} L^{-1} was calculated over the final 3-hour pilot-scale experimental period when the WAS temperature stabilized at ca. 63 °C (see Fig. 10a). The additional heat required to raise the WAS temperature to 60 °C was estimated at 1672 MWh, according to Eq. (7) (adapted from Budych-Gorzna et al. [78]):

$$H_{demand} = \frac{\Delta T \times V \times \rho \times C_P}{3600} \quad (7)$$

where H_{demand} is the total heat energy required per year (kWh), ΔT is the temperature increase (°C), V is the annual volume of WAS produced (m^3), ρ and C_P is the density and specific heat of water (assumed similar for sludge, 1000 kg m^{-3} and 4.18 kJ $kg^{-1}.°C^{-1}$), respectively, and the factor 3600 is used to convert kJ to kWh (since 1 kWh = 3600 kJ).

The required CPC area (A_{CPC}, m^2) for each scenario was calculated through Eq. (8), based on the accumulated UV energy demand (Q_{UV}, kJ L^{-1}) and the yearly solar accumulated UV energy (E_y) recorded in Porto, Portugal during 2023–274,662 kJ m^{-2} (source: IPMA [29]), and the yearly volume of WAS (V_Y) processed by a WWTP serving 300,000 people, totalling 36,000 m^3.

$$A_{CPC} = \frac{Q_{UV} \times V_Y \times 1000}{E_Y} \quad (8)$$

Given the vast difference in the Q_{UV} values, Scenario 2 presents a marked 58 % reduction in the required CPC area. Specifically, total CPC areas needed for Scenarios 1 and 2 were estimated at 3759 and 1585 m^2, respectively (Table 2), corresponding to land areas of 14,867 and 6375 m^2 for CPCs full-scale implementation. These land requirements consider the optimal orientation and tilt of the CPC modules, which are south-oriented (appropriate for the Northern Hemisphere) and tilted at an angle of 41° to match the local latitude of Porto, ensuring optimal capture of solar photons. Additionally, the land allocation considers the individual module size of 2.04 m^2 and an inter-row spacing of 3.94 m, determined by the sun's lowest elevation angle of 26°, to minimize shading. This arrangement means each 2.04 m^2 CPC module effectively occupies 5.55 m^2 of land (Table SM-3).

The overall costs of the full-scale WAS pre-treatment plant were estimated based on literature sources [93,94]. The expenses include solar-thermal facilities, system engineering and assembly, project contingencies, maintenance material, spare parts, and electric supply. The cost associated with the installation of CPCs was calculated as a function of their area, following the pricing guidelines reported by Lillo-Bravo et al. [94]. Specifically: (i) for areas ≤50 m^2, the CPC cost is 325 € per m^2; and (ii) for areas ≥2000 m^2, the CPC cost is reduced to 225 € per m^2. For Scenario 2, where the required CPC area falls between these two ranges, costs were interpolated, resulting in a 54 % reduction compared to Scenario 1, which demanded a 2.4-fold higher area.

However, it is important to note that Scenario 2 also necessitates additional investments in a heat exchanger and incurs extra operating costs for the electricity needed to pre-heat the WAS. These additional expenses were carefully considered in the economic evaluation (Table 3), as they impact the total cost-effectiveness and feasibility of the pre-treatment plant setup.

The total yearly cost (TYC) for the WAS pre-treatment via solar-assisted thermal process was determined by summing the annual capital cost – which is derived by multiplying the total capital requirement (TCR) by the fixed charge rate (FCR) – with the operating costs (OC), as outlined in Eq. (9) [93]. This formula integrates initial capital investments, and the recurring expenditures required to operate the pre-treatment facility effectively, providing a comprehensive overview of

Table 3
Comparative cost analysis for full-scale WAS solar-assisted thermal pre-treatment operating without (Scenario 1) and with (Scenario 2) external heating.

Target Q_{UV} ($kJ\,L^{-1}$)	Scenario 1	Scenario 2
	28.7	12.1
Direct cost:		
CPC area (m^2)	3759	1585
A - Total collector cost (€)	845,706	389,863
B - Piping and tanks (8 % of A, €)	67,656	31,189
C - Auxiliary equipment and controls (10 % of A, €)	84,571	38,986
D - Others (15 % of A, €)	126,856	58,479
E - Heat exchanger (€)	0	45,000[a]
Total direct cost (TDC = A + B + C + D + E) (€)	1,124,788	563,518
Indirect cost:		
F - Contingencies (12 % of TDC, €)	134,975	67,622
G - Spare parts (1 % of TDC, €)	11,248	5635
Total capital required (TCR = TDC + F + G) (€)	1,271,011	636,775
Yearly cost:		
H - Capital (12 % of TCR, 20 years, €)	152,521	76,413
I - Operation and maintenance (2 % and 1.5 % of TDC, €)	22,496	8453
J - Electricity cost with the heat exchanger (€)	0	234,080[b]
K - Replacement costs (10 % of TDC, €)	112,479	56,352
Total yearly cost (TYC = H + I + J + K) (€)	**287,496**	**375,297**
Unitary cost (UC = TYC/V) (€ m^{-3})	**8**	**10.4**

[a] Value obtained from Caetano [95].
[b] Assuming 0.14 €/kWh as the electricity cost [96].

the annual financial commitments.

$$TYC = TCR \times FCR + OC \quad (9)$$

The TCR encompasses both direct costs (e.g., piping, tanks, auxiliary equipment, control systems) and indirect costs (e.g., contingencies and spare parts), all integral to the initial investment of the solar-thermal facility. The FCR was estimated at 12 %, calculated based on a 20-year plant depreciation period [93,94]. This rate reflects the annual financial commitment necessary to cover the capital outlay, amortisation, and other related financial obligations over the expected lifespan of the facility.

While Scenario 1 requires a higher upfront investment due to the larger CPC area, with a total capital requirement twice as high as Scenario 2, the latter incurs significantly greater operational costs, primarily driven by electricity consumption for sludge pre-heating, which accounts for nearly 62 % of the total yearly cost (Table 3). Although the additional investment in a heat exchanger (€45,000) in Scenario 2 is offset by savings related to the collector costs, the annual heat demand (1672 MWh) outweighs the benefits gained from the 58 % reduction in CPC area, ultimately diminishing its economic feasibility under current electricity prices. These findings highlight the critical balance between operational and capital expenditures in WAS pre-treatment systems. When combining both costs, Scenario 1 achieves a 23 % reduction in the total yearly cost compared to Scenario 2, amounting to 87,802 € in savings, and reduces the unitary pre-treatment cost from 10.4 to 8.0 € m^{-3} of pre-treated WAS. Therefore, despite its higher capital requirement, Scenario 1 – relying only on solar radiation – offers a more sustainable and cost-effective long-term solution, particularly in regions with abundant sunlight, where solar-driven pre-treatment can enhance both energy efficiency and economic viability. Notwithstanding, while Scenario 2 – combining solar radiation with external heating – is less cost-effective on a per-unit basis, this hybrid approach may still be viable if renewable energy sources can offset energy costs or if land constraints limit the installation of the CPC field.

Furthermore, incorporating complementary technologies could further enhance energy recovery and resource valorisation while reducing environmental impacts and improving overall process sustainability and efficiency through: (i) carbon capture and utilisation (CCU) to convert CO_2 from biogas upgrading into additional methane; (ii) repurposing treated sludge for agricultural applications, either as fertiliser or for biochar production; and (iii) recovering nutrients, particularly nitrogen and phosphorus, from the drainage water from the sludge treatment [97–99]. By increasing methane production through pre-treatment and integrating energy recovery measures, WWTPs can move toward self-sufficiency while aligning with Sustainable Development Goals (SDGs).

Specifically, the process supports SDG 6 by promoting more efficient and sustainable wastewater management, consistent with Target 6.3, which aims to improve water quality and reduce pollution through better treatment practices. It also contributes to SDG 7, particularly Target 7.2, by increasing the share of renewable energy in the energy mix through the use of solar radiation in the pre-treatment process. Additionally, by enhancing the valorisation of sludge and reducing waste generation, the study supports SDG 12, in line with Target 12.5, which focuses on substantially reducing waste generation through prevention, reduction, and recycling strategies [100]. Thus, the proposed approach not only improves process performance but also reinforces the principles of environmental responsibility and circular resource use.

4. Conclusion

This study demonstrates that the synergy between low-temperature pre-treatment and solar radiation in a tubular photoreactor provides a clear benefit, as both mechanisms significantly enhance WAS disintegration and boost methane production.

Laboratory-scale experiments, combining simulated sunlight with external heating, showed a substantial increase in methane production for pre-treated WAS compared to the untreated control sample, ranging from 32 % to 74 % as the pre-treatment temperature increased from 50 °C to 70 °C, following an accumulated UV energy of 7.6 kJ_{UV} L^{-1} (radiant power of 0.66 W_{UV} for 3 h). A radiant power of 0.66 W_{UV} proved optimal for COD solubilization, achieving maximum cellular damage, with no further improvement at higher radiation intensities (e.g., 0.83 W_{UV}). Although reflector geometry had minimal impact on WAS hydrolysis, further research on flat reflective surfaces is recommended for large-scale applications, especially from an economic perspective.

Pilot-scale experiments reinforced the laboratory findings, demonstrating an 84.9 % increase in methane production following a 7-hour solar-driven pre-treatment conducted under natural sunlight (28.7 kJ_{UV} L^{-1}) without external heating. In the “Sunlight” experiment, solar radiation alone elevated WAS temperature to 63 °C during the first 4 h (accumulating 16.6 kJ_{UV} L^{-1}) and maintained that temperature for an additional 3 h (adding 12.1 kJ_{UV} L^{-1}).

The economic assessment revealed that WAS pre-treatment relying only on natural solar radiation (Scenario 1; 28.7 kJ_{UV} L^{-1}) is more economically viable (8.0 vs. 10.4 € m^{-3}) than a system that incorporates sunlight harvesting devices with external heating (Scenario 2; 12.1 kJ_{UV} L^{-1}; 1672 MWh). Although external heating reduces the required CPC area, its high electricity demand accounts for a significant portion of the total yearly cost (62 %), ultimately diminishing economic feasibility under current energy prices. These findings highlight the critical balance between capital and operational expenditures in WAS solar-assisted thermal pre-treatment systems and suggest that solar-based pre-treatment is most advantageous in regions with abundant sunlight. In areas with low sunlight, the reduced solar input would weaken the synergistic effect with thermal energy, requiring greater reliance on external heating sources. This would increase costs and diminish both the economic and environmental benefits.

While the pilot-scale results demonstrate the potential for larger-scale implementation, further studies are needed to address practical challenges such as energy efficiency, reactor design, and performance under variable weather conditions. At a more advanced stage, when applicable, a comprehensive life cycle assessment (LCA) could also be incorporated to evaluate the overall environmental impact and sustainability of the proposed pre-treatment strategy.

CRediT authorship contribution statement

Joana P. Monteiro: Writing – original draft, Investigation, Formal analysis. **Tânia F.C.V. Silva:** Writing – review & editing, Formal analysis. **Catarina Cruzeiro:** Writing – review & editing, Formal analysis. **M. Salomé Duarte:** Writing – review & editing, Formal analysis. **M. Alcina Pereira:** Writing – review & editing, Supervision, Conceptualization. **Vítor J.P. Vilar:** Writing – review & editing, Supervision, Conceptualization.

Declaration of competing interest

The authors declare that they have no known competing financial interests or personal relationships that could have appeared to influence the work reported in this paper.

Acknowledgments

This research was also supported by national funds through FCT/MCTES (PIDDAC): LSRE-LCM - UIDB/50020/2020 (DOI: 10.54499/UIDB/50020/2020) and UIDP/50020/2020 (DOI: 10.54499/UIDP/50020/2020); and ALiCE - LA/P/0045/2020 (DOI: 10.54499/LA/P/0045/2020); and under the scope of the strategic funding of UIDB/04469/2020 unit (DOI: 10.54499/UIDB/04469/2020), and by LABBELS – Associate Laboratory in Biotechnology, Bioengineering and Microelectromechanical Systems, LA/P/0029/2020.

The first author acknowledges her PhD scholarship supported by FCT, 2020.04887.BD (DOI: 10.54499/2020.04887.BD). The second author acknowledges FCT Individual Call to Scientific Employment Stimulus 2017 (CEECIND/01386/2017 – DOI: 10.54499/CEECIND/01386/2017/CP1399/CT0011). The third author acknowledges her fellowship from the "la Caixa" Foundation (ID 100010434), with the code LCF/BQ/PI23/11970038. The fourth author acknowledges FCT for the Junior Research contract obtained under the scope of the Scientific Stimulus Employment 2022 (2022.06569.CEECIND – DOI 2022.06569.CEECIND/CP1718/CT0004). The sixth author acknowledges the FCT Individual Call to Scientific Employment Stimulus 2017 (CEECIND/01317/2017 – DOI: 10.54499/CEECIND/01317/2017/CP1399/CT0010).

Appendix A. Supplementary data

Supplementary data to this article can be found online at https://doi.org/10.1016/j.cej.2025.166416.

Data availability

Data will be made available on request.

References

[1] Shiyang Li, et al., Regulating secretion of extracellular polymeric substances through dosing magnetite and zerovalent iron nanoparticles to affect anaerobic digestion mode, ACS Sustain. Chem. Eng. 7 (10) (2019) 9655–9662, https://doi.org/10.1021/acssuschemeng.9b01252.
[2] R.B. Sowby, Making waves: research to support water and wastewater utilities in the transition to a clean-energy future, Water Res. 233 (2023) 119739, https://doi.org/10.1016/j.watres.2023.119739.
[3] A. Strazzabosco, et al., Expert opinion on influential factors driving renewable energy adoption in the water industry, Renew. Energy 162 (2020) 754–765, https://doi.org/10.1016/j.renene.2020.08.054.
[4] Commision, European, REPowerEU. https://commission.europa.eu/strategy-and-policy/priorities-2019-2024/european-green-deal/repowereu-affordable-secure-and-sustainable-energy-europe_en#documents, 2022.
[5] Union, European Parliament and Council of the European. Directive (EU) 2024/3019 of the European Parliament and of the Council of 27 November 2024 concerning urban wastewater treatment. 2024/3019. 2024. https://eur-lex.europa.eu/legal-content/EN/TXT/PDF/?uri=OJ:L_202403019.
[6] Mariana Cardoso Chrispim, Miklas Scholz, and Marcelo Antunes Nolasco, *biogas recovery for sustainable cities: a critical review of enhancement techniques and key local conditions for implementation*, Sustain. Cities Soc. 72 (2021) 103033, https://doi.org/10.1016/j.scs.2021.103033.
[7] Elena C. Blanco, Mariano Martín, Pastora Vega, Achieving energy self-sufficiency in wastewater treatment plants by integrating municipal solid waste treatment: a process design study in Spain, J. Environ. Chem. Eng. 11 (5) (2023) 110673, https://doi.org/10.1016/j.jece.2023.110673.
[8] A. Gonzalez, et al., Pre-treatments to enhance the biodegradability of waste activated sludge: elucidating the rate limiting step, Biotechnol. Adv. 36 (5) (2018) 1434–1469, https://doi.org/10.1016/j.biotechadv.2018.06.001.
[9] V. Khanh Nguyen, et al., Review on pretreatment techniques to improve anaerobic digestion of sewage sludge, Fuel 285 (2021) 119105, https://doi.org/10.1016/j.fuel.2020.119105.
[10] Ivet Ferrer, et al., Increasing biogas production by thermal (70 C) sludge pre-treatment prior to thermophilic anaerobic digestion, Biochem. Eng. J. 42 (2) (2008) 186–192, https://doi.org/10.1016/j.bej.2008.06.020.
[11] Tianlong Zheng, et al., Effects of low-and high-temperature thermal-alkaline pretreatments on anaerobic digestion of waste activated sludge, Bioresour. Technol. 337 (2021) 125400, https://doi.org/10.1016/j.biortech.2021.125400.
[12] Guangyin Zhen, et al., Overview of pretreatment strategies for enhancing sewage sludge disintegration and subsequent anaerobic digestion: current advances, full-scale application and future perspectives, Renew. Sustain. Energy Rev. 69 (2017) 559–577, https://doi.org/10.1016/j.rser.2016.11.187.
[13] Katarzyna Bułkowska, Magdalena Zielińska, Thermal disintegration of waste-activated sludge, Energies 17 (17) (2024) 4447 (https://www.mdpi.com/1996-1073/17/17/4447).
[14] Qiandi Wang, et al., Mechanistic insights into the effects of biopolymer conversion on macroscopic physical properties of waste activated sludge during hydrothermal treatment: importance of the Maillard reaction, Sci. Total Environ. 769 (2021) 144798, https://doi.org/10.1016/j.scitotenv.2020.144798.
[15] Wangwang Yan, et al., Effects of sludge thermal hydrolysis pretreatment on anaerobic digestion and downstream processes: mechanism, challenges and solutions, Bioresour. Technol. 344 (2022) 126248, https://doi.org/10.1016/j.biortech.2021.126248.
[16] B. Ruffino, et al., Improvement of anaerobic digestion of sewage sludge in a wastewater treatment plant by means of mechanical and thermal pre-treatments: performance, energy and economical assessment, Bioresour. Technol. 175 (2015) 298–308, https://doi.org/10.1016/j.biortech.2014.10.071.
[17] Hélène Carrere, et al., Pretreatment methods to improve sludge anaerobic degradability: a review, J. Hazard. Mater. 183 (2010) 1–15, https://doi.org/10.1016/j.jhazmat.2010.06.129.
[18] Audrey Prorot, et al., Sludge disintegration during heat treatment at low temperature: a better understanding of involved mechanisms with a multiparametric approach, Biochem. Eng. J. 54 (3) (2011) 178–184, https://doi.org/10.1016/j.bej.2011.02.016.
[19] Joana P. Monteiro, et al., Innovative waste activated sludge pre-treatment using a raceway pond reactor: integration of low-temperature and solar radiation, Chem. Eng. J. 498 (2024) 155324, https://doi.org/10.1016/j.cej.2024.155324.
[20] Sixto Malato, et al., Decontamination and disinfection of water by solar photocatalysis: the pilot plants of the Plataforma solar de Almeria, Mater. Sci. Semicond. Process. 42 (2016) 15–23, https://doi.org/10.1016/j.mssp.2015.07.017.
[21] Karen Sofía Ochoa-Gutiérrez, et al., A novel prototype offset multi tubular Photoreactor (OMTP) for solar photocatalytic degradation of water contaminants, Chem. Eng. J. 341 (2018) 628–638, https://doi.org/10.1016/j.cej.2018.02.068.
[22] Rowan J. Braham, Andrew T. Harris, Review of major design and scale-up considerations for solar photocatalytic reactors, Ind. Eng. Chem. Res. 48 (19) (2009) 8890–8905, https://doi.org/10.1021/ie900859z.
[23] Sixto Malato, et al., Photocatalytic decontamination and disinfection of water with solar collectors, Catal. Today 122 (1) (2007) 137–149, https://doi.org/10.1016/j.cattod.2007.01.034.
[24] Bruna Porto, et al., Tubular photobioreactors illuminated with LEDs to boost microalgal biomass production, Chem. Eng. J. 435 (2022) 134747, https://doi.org/10.1016/j.cej.2022.134747.
[25] Dawei Wang, et al., Engineering and modeling perspectives on photocatalytic reactors for water treatment, Water Res. 202 (2021) 117421, https://doi.org/10.1016/j.watres.2021.117421.
[26] Ana I. Gomes, et al., Cost-effective solar collector to promote photo-Fenton reactions: a case study on the treatment of urban mature leachate, J. Clean. Prod. 199 (2018) 369–382, https://doi.org/10.1016/j.jclepro.2018.07.113.
[27] R. Uma Rani, et al., Low temperature thermo-chemical pretreatment of dairy waste activated sludge for anaerobic digestion process, Bioresour. Technol. 103 (1) (2012) 415–424, https://doi.org/10.1016/j.biortech.2011.09.124.
[28] Chin Seng Liew, et al., Hydrolysis kinetics for solubilizing waste activated sludge at low temperature thermal treatment derived from multivariate non-linear model, Chemosphere 292 (2022) 133478, https://doi.org/10.1016/j.chemosphere.2021.133478.
[29] Atmosfera, Instituto Português do Mar e da. Instituto Português do Mar e da Atmosfera. 2024; Available from: https://www.ipma.pt/pt/index.html.
[30] Ismael L. Lozano, Inmaculada Alados, Inmaculada Foyo-Moreno, Analysis of the solar radiation/atmosphere interaction at a Mediterranean site: the role of clouds, Atmos. Res. 296 (2023) 107072, https://doi.org/10.1016/j.atmosres.2023.107072.
[31] C.G. Hatchard, And C a_ Parker, *a new sensitive chemical actinometer-II. Potassium ferrioxalate as a standard chemical actinometer*. Proceedings of the Royal Society of London. Series A, Mathematical and Physical Sciences 235 (1203) (1956) 518–536, https://doi.org/10.1098/rspa.1956.0102.
[32] Miguel Rios-Enriquez, et al., Optimization of the heterogeneous Fenton-oxidation of the model pollutant 2,4-xylidine using the optimal experimental design methodology, Solar Energy 77 (5) (2004) 491–501, https://doi.org/10.1016/j.solener.2004.03.027.
[33] Adrian Gonzalez, et al., Mild thermal pre-treatment of waste activated sludge to increase loading capacity, biogas production, and solids' degradation: a pilot-scale study, Energies 13 (22) (2020) 6059, https://doi.org/10.3390/en13226059.
[34] APHA, *Standard methods for the examination of water and wastewater*. American Public Health Association (APHA), American Water Works Association (AWWA) and Water Environment Federation (WEF), 2012. 22nd edition.
[35] X.Y. Li, S.F. Yang, Influence of loosely bound extracellular polymeric substances (EPS) on the flocculation, sedimentation and dewaterability of activated sludge, Water Res. 41 (5) (2007) 1022–1030, https://doi.org/10.1016/j.watres.2006.06.037.
[36] Probes, Invitrogen Molecular. Invitrogen molecular probes LIVE/DEAD® BacLight bacterial viability kits, in L7012. 2014.
[37] Standardization), ISO (the International Organization for, *ISO 4831:2006*, in *Microbiology of food and animal feeding stuffs — Horizontal method for the detection and enumeration of coliforms — Most probable number technique*. 2021.
[38] I. Angelidaki, et al., Defining the biomethane potential (BMP) of solid organic wastes and energy crops: a proposed protocol for batch assays, Water Sci. Technol. 59 (5) (2009) 927–934, https://doi.org/10.2166/wst.2009.040.
[39] Christof Holliger, et al., Towards a Standardization of Biomethane Potential Tests, Water Science & Technology, 2016, p. 74, https://doi.org/10.2166/wst.2016.336.
[40] Huan Li, et al., Optimized alkaline pretreatment of sludge before anaerobic digestion, Bioresour. Technol. 123 (2012) 189–194, https://doi.org/10.1016/j.biortech.2012.08.017.
[41] J.C. Costa, et al., Biomethanation potential of macroalgae Ulva spp. and Gracilaria spp. and in co-digestion with waste activated sludge, Bioresour. Technol. 114 (2012) 320–326, https://doi.org/10.1016/j.biortech.2012.03.011.

[42] Blatchley III, ER, et al., Bacterial Responses to Ultraviolet Irradiation. Water Science and Technology, 2001. vol. 43(10): p. 179–186 DOI:https://doi.org/10.2166/wst.2001.0614.

[43] María Castro-Alférez, et al., Mechanistic model of the Escherichia coli inactivation by solar disinfection based on the photo-generation of internal ROS and the photo-inactivation of enzymes: CAT and SOD, Chem. Eng. J. 318 (2017) 214–223, https://doi.org/10.1016/j.cej.2016.06.093.

[44] María Castro-Alférez, et al., Mechanistic modeling of UV and mild-heat synergistic effect on solar water disinfection, Chem. Eng. J. 316 (2017) 111–120, https://doi.org/10.1016/j.cej.2017.01.026.

[45] María Castro-Alférez, et al., Mechanistic model of the Escherichia coli inactivation by solar disinfection based on the photo-generation of internal ROS and the photo-inactivation of enzymes: CAT and SOD, Chem. Eng. J. (2016) 318, https://doi.org/10.1016/j.cej.2016.06.093.

[46] Colón, Joan, et al., *Producing sludge for agricultural applications*. 2017, DOI:https://doi.org/10.2166/9781780407876_0296.

[47] Matthew Dryden, Reactive oxygen therapy: a novel therapy in soft tissue infection, Curr. Opin. Infect. Dis. 30 (2) (2017) 143–149.

[48] Michael M. Gaschler, Brent R. Stockwell, Lipid peroxidation in cell death, Biochem. Biophys. Res. Commun. 482 (3) (2017) 419–425, https://doi.org/10.1016/j.bbrc.2016.10.086.

[49] Michael P. Murphy, et al., *Guidelines for measuring reactive oxygen species and oxidative damage in cells and in vivo*. Nature, Metabolism 4 (6) (2022) 651–662, https://doi.org/10.1038/s42255-022-00591-z.

[50] Stefanos Giannakis, et al., Solar disinfection is an augmentable, in situ-generated photo-Fenton reaction-part 1: a review of the mechanisms and the fundamental aspects of the process, Appl. Catal. Environ. 199 (2016) 199–223, https://doi.org/10.1016/j.apcatb.2016.06.009.

[51] Kun Luo, et al., Hydrolysis kinetics in anaerobic digestion of waste activated sludge enhanced by α-amylase, Biochem. Eng. J. 62 (2012) 17–21, https://doi.org/10.1016/j.bej.2011.12.009.

[52] Kristjansson, Jakob and Stetter, Karl. Thermophilic Bacteria. 2020. p. 1-18, https://doi.org/10.1201/9781003068334-1.

[53] Yinguang Chen, et al., Hydrolysis and acidification of waste activated sludge at different pHs, Water Res. 41 (3) (2007) 683–689, https://doi.org/10.1016/j.watres.2006.07.030.

[54] Yonggang Xue, et al., Effects of thermal hydrolysis on organic matter solubilization and anaerobic digestion of high solid sludge, Chem. Eng. J. 264 (2015) 174–180, https://doi.org/10.1016/j.cej.2014.11.005.

[55] Mariusz Kuglarz, Dimitar Karakashev, and Irini Angelidaki, *microwave and thermal pretreatment as methods for increasing the biogas potential of secondary sludge from municipal wastewater treatment plants*, Bioresour. Technol. 134 (2013) 290–297, https://doi.org/10.1016/j.biortech.2013.02.001.

[56] Ivo Nges, Jing Liu, Effects of anaerobic pre-treatment on the degradation of dewatered-sewage sludge, Renew. Energy 34 (2009) 1795–1800, https://doi.org/10.1016/j.renene.2008.12.001.

[57] Lise Appels, et al., Influence of low temperature thermal pre-treatment on sludge solubilisation, heavy metal release and anaerobic digestion, Bioresour. Technol. 101 (15) (2010) 5743–5748, https://doi.org/10.1016/j.biortech.2010.02.068.

[58] Harrison, Susan T. L. *2.44 – Cell Disruption*. 2011.

[59] Elisabeth Neyens, Jan Baeyens, Raf Dewil, Advanced sludge treatment affects extracellular polymeric substances to improve activated sludge dewatering, J. Hazard. Mater. 106 (2–3) (2004) 83–92, https://doi.org/10.1016/j.jhazmat.2003.11.014.

[60] Pan Zhou, et al., Comparison of different sewage sludge pretreatment technologies for improving sludge solubilization and anaerobic digestion efficiency: a comprehensive review, Sci. Total Environ. 921 (2024) 171175, https://doi.org/10.1016/j.scitotenv.2024.171175.

[61] Xiyao Li, et al., Anaerobic digestion using ultrasound as pretreatment approach: changes in waste activated sludge, anaerobic digestion performances and digestive microbial populations, Biochem. Eng. J. 139 (2018) 139–145, https://doi.org/10.1016/j.bej.2017.11.009.

[62] Kaixin Zheng, et al., Enhanced methane production from anaerobic digestion of waste activated sludge by combining ultrasound with potassium permanganate pretreatment, Sci. Total Environ. 857 (2023) 159331, https://doi.org/10.1016/j.scitotenv.2022.159331.

[63] Phuong Linh Ngo, et al., Mechanisms, status, and challenges of thermal hydrolysis and advanced thermal hydrolysis processes in sewage sludge treatment, Chemosphere 281 (2021) 130890, https://doi.org/10.1016/j.chemosphere.2021.130890.

[64] Benyi Xiao, et al., Evaluation of the microbial cell structure damages in alkaline pretreatment of waste activated sludge, Bioresour. Technol. 196 (2015) 109–115, https://doi.org/10.1016/j.biortech.2015.07.056.

[65] X. Shi, et al., Surfactant-assisted thermal hydrolysis off waste activated sludge for improved dewaterability, organic release, and volatile fatty acid production, Waste Manag. 124 (2021) 339–347, https://doi.org/10.1016/j.wasman.2021.02.024.

[66] Xiaohu Dai, et al., Degradation of extracellular polymeric substances (EPS) in anaerobic digestion of dewatered sludge, Procedia Environ. Sci. 18 (2013) 515–521, https://doi.org/10.1016/j.proenv.2013.04.069.

[67] D.I. Pattison, M.J. Davies, Actions of ultraviolet light on cellular structures, in: Exs, 2006, pp. 131–157, https://doi.org/10.1007/3-7643-7378-4_6.

[68] Li, Y.Y. and T. Noike, Upgrading of Anaerobic Digestion of Waste Activated Sludge by Thermal Pretreatment. Water Science and Technology, 1992. vol. 26 (3–4): p. 857–866 DOI:https://doi.org/10.2166/wst.1992.0466.

[69] Blanca Ibáñez, et al., Molecular insights into radiation effects and protective mechanisms: a focus on cellular damage and Radioprotectors. Current issues, Mol. Biol. 46 (11) (2024) 12718–12732 (https://www.mdpi.com/1467-3045/46/11/755).

[70] Kumar Biswal, Basanta, et al., Impact of low-thermal pretreatment on physicochemical properties of saline waste activated sludge, hydrolysis of organics and methane yield in anaerobic digestion, Bioresour. Technol. 297 (2020) 122423, https://doi.org/10.1016/j.biortech.2019.122423.

[71] Xuemei Zou, et al., Effects of mixed alkali-thermal pretreatment on anaerobic digestion performance of waste activated sludge, J. Clean. Prod. 259 (2020) 120940, https://doi.org/10.1016/j.jclepro.2020.120940.

[72] Ziyi Yang, et al., Mitigation of ammonia inhibition through bioaugmentation with different microorganisms during anaerobic digestion: selection of strains and reactor performance evaluation, Water Res. 155 (2019) 214–224, https://doi.org/10.1016/j.watres.2019.02.048.

[73] Orhan Yenigün, Burak Demirel, Ammonia inhibition in anaerobic digestion: a review, Process Biochem. 48 (5) (2013) 901–911, https://doi.org/10.1016/j.procbio.2013.04.012.

[74] Matías Olivera, et al., Effects of short retention times and ultrasound pretreatment on ammonium concentration and organic matter transformation in anaerobic digesters treating sewage sludge, Fermentation 10 (1) (2024) 63, https://doi.org/10.3390/fermentation10010063.

[75] Claire Bougrier, Jean Philippe Delgenès, and Hélène Carrère, *effects of thermal treatments on five different waste activated sludge samples solubilisation, physical properties and anaerobic digestion*, Chem. Eng. J. 139 (2) (2008) 236–244, https://doi.org/10.1016/j.cej.2007.07.099.

[76] Nervana Haffiez, et al., Propagation of antibiotic resistance genes during anaerobic digestion of thermally hydrolyzed sludge and their correlation with extracellular polymeric substances, Sci. Rep. 12 (1) (2022) 6749, https://doi.org/10.1038/s41598-022-10764-1.

[77] Nicky Eshtiaghi, et al., Rheological characterisation of municipal sludge: a review, Water Res. 47 (15) (2013) 5493–5510, https://doi.org/10.1016/j.watres.2013.07.001.

[78] Ehsan Farno, et al., Rheological characterisation of thermally-treated anaerobic digested sludge: impact of temperature and thermal history, Water Res. 51 (2014) 156–161, https://doi.org/10.1016/j.watres.2014.02.048.

[79] José L. Urrea, et al., *Rheological behaviour of activated sludge treated by thermal hydrolysis*. Journal of water, Process. Eng. 5 (2015) 153–159, https://doi.org/10.1016/j.jwpe.2014.06.009.

[80] Ruikun Wang, et al., Effects of the low-temperature thermo-alkaline method on the rheological properties of sludge, J. Environ. Manage. 177 (2016) 74–83, https://doi.org/10.1016/j.jenvman.2016.04.021.

[81] Guohong Feng, Yabing Guo, Wei Tan, Effects of thermal hydrolysis temperature on physical characteristics of municipal sludge, Water Sci. Technol. 72 (11) (2015) 2018–2026, https://doi.org/10.2166/wst.2015.425.

[82] Yingjun Zhou, et al., Effect of thermal hydrolysis pre-treatment on anaerobic digestion of municipal biowaste: a pilot scale study in China, J. Biosci. Bioeng. 116 (1) (2013) 101–105, https://doi.org/10.1016/j.jbiosc.2013.01.014.

[83] S. Miryahyaei, et al., Impact of rheological properties of substrate on anaerobic digestion and digestate dewaterability: new insights through rheological and physico-chemical interaction, Water Res. 150 (2019) 56–67, https://doi.org/10.1016/j.watres.2018.11.049.

[84] Jibao Liu, et al., A comprehensive insight into the effects of microwave-H2O2 pretreatment on concentrated sewage sludge anaerobic digestion based on semi-continuous operation, Bioresour. Technol. 256 (2018) 118–127, https://doi.org/10.1016/j.biortech.2018.01.126.

[85] Y. Li, et al., Enhancing the quantity and quality of short-chain fatty acids production from waste activated sludge using CaO2 as an additive, Water Res. 83 (2015) 84–93, https://doi.org/10.1016/j.watres.2015.06.021.

[86] Xavier Bonjoch, A.R. Blanch, Resistance of faecal coliforms and enterococci populations in sludge and biosolids to different hygienisation treatments, Microb. Ecol. 57 (2009) 478–483, https://doi.org/10.1007/s00248-008-9430-7.

[87] EPA, Standards for the Use or Disposal of Sewage Sludge (40 CFR Part 503), 1993.

[88] Adel A.S. AL-Gheethi, et al., Reduction of faecal indicators and elimination of pathogens from sewage treated effluents by heat treatment, Caspian J. Appl. Sci. Res. 2 (2) (2013).

[89] M. Rojas Oropeza, et al., Removal of fecal indicator organisms and parasites (fecal coliforms and helminth eggs) from municipal biologic sludge by anaerobic mesophilic and thermophilic digestion, Water Sci. Technol. 44 (4) (2001) 97–101, https://doi.org/10.2166/wst.2001.0189.

[90] Chuan Jiang, et al., A review of the compound parabolic concentrator (CPC) with a tubular absorber, Energies 13 (3) (2020) 695, https://doi.org/10.3390/en13030695.

[91] Ionel Rosenthal, in: I. Rosenthal (Ed.), *Infrared Radiation*, in *Electromagnetic Radiations in Food Science*, Springer, Berlin Heidelberg: Berlin, Heidelberg, 1992, pp. 105–114, https://doi.org/10.1007/978-3-642-77106-4_4.

[92] Carla Balocco, et al., Experimental transmittance of polyethylene films in the solar and infrared wavelengths, Sol. Energy 165 (2018) 199–205, https://doi.org/10.1016/j.solener.2018.03.011.

[93] Tânia F.C.V. Silva, et al., Scale-up and cost analysis of a photo-Fenton system for sanitary landfill leachate treatment, Chem. Eng. J. 283 (2016) 76–88, https://doi.org/10.1016/j.cej.2015.07.063.

[94] Isidoro Lillo-Bravo, et al., Benefits of medium temperature solar concentration technologies as thermal energy source of industrial processes in Spain, Energies 11 (11) (2018) 2950, https://doi.org/10.3390/en11112950.

[95] Ana Maria Teixeira Caetano, Recuperação do Calor de um Efluente Primário para Aquecimento de Lamas de um Reactor Anaeróbio, Instituto Superior de Engenharia do Porto, 2011, p. 40. Available from: https://recipp.ipp.pt/bitstream/10400.22/2519/1/DM_AnaCaetano_2011_MEQ.pdf https://recipp.ipp.pt/bitstream/10400.22/2519/1/DM_AnaCaetano_2011_MEQ.pdf.
[96] Santos, Fundação Francisco Manuel dos. Pordata. 2025; Available from: https://www.pordata.pt/pt.
[97] Wei Wang, Jo-Shu Chang, Duu-Jong Lee, Anaerobic digestate valorization beyond agricultural application: current status and prospects, Bioresour. Technol. 373 (2023) 128742, https://doi.org/10.1016/j.biortech.2023.128742.
[98] Serhiy Marchuk, et al., Biosolids-derived fertilisers: a review of challenges and opportunities, Sci. Total Environ. 875 (2023) 162555, https://doi.org/10.1016/j.scitotenv.2023.162555.
[99] Stephanie S. Cordova, et al., What should we do with CO_2 from biogas upgrading? J CO_2 Util 77 (2023) 102607 https://doi.org/10.1016/j.jcou.2023.102607.
[100] Assembly, United Nations General, Transforming our world: the 2030 agenda for sustainable development, U. Nations, 2015. https://docs.un.org/en/A/RES/70/1.